Investigation of Seismo-Ionospheric Anomalies before large Earthquakes during 2001-2018

Rukhshinda Aftab

M.Phil. Geophysics

(2020-2022)
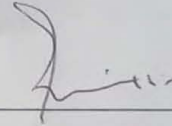
Department of Earth Sciences

Quaid-i-Azam, University Islamabad.

CERTIFICATE

It is certified that **Ms. Rukhshinda Aftab D/o Said Aman Shah (Registration No. 02112013003)** carried out the work contained in this dissertation under my supervision and accepted in its present form by Department of Earth Sciences as satisfying the requirements for the award of **M.Phil Degree in Geophysics.**
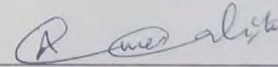
RECOMMENDED BY

Dr. Anees Ahmad Bangash
Assistant Professor/Supervisor

Dr. M. Gulraiz Akhter
External Examiner

Dr. Aamir Ali
Chairperson

DEPARTMENT OF EARTH SCIENCES
QUAID-I-AZAM UNIVERSITY
ISLAMABAD

Dedication

I would love to dedicate this work to myself for going against

odds.

Acknowledgement

ABSTRACT

Advances in space and remote sensing have contributed highly to the concept of lithosphere-atmosphere-ionosphere coupling over earthquake active zone. For the identification of ionospheric perturbations linked to earthquakes, Total Electron Content (TEC) data has been retrieved from Global position system stations within Dobrovolsky's radius. This research has been conducted for 10 shallow-depth earthquakes worldwide with a magnitude greater than 7 from 2001 to 2018. The TEC changes have been observed for 15 days before and 10 days after the main shock with the condition of the day being geomagnetically quite (KP<40 & Dst>-50nT). Nine out of ten earthquakes exhibit substantial Total Electron Content (TEC) features within a window of one to eleven days, and these anomalies disappear after the earthquake occurrence, which is consistent with the forecasted outcomes. Among which six earthquakes have anomalous values of TEC two days before the main shock, three earthquake showed anomalies eleven days prior while four earthquakes gives ionospheric anomalies six days prior to the earthquakes. Likewise, the land surface temperature (LST) plot for one earthquake as secondary data has also proven to show temperature variation four days before the earthquake on the epicenter. The discharge of a significant amount of energy from the epicenter during the EQ preparation period may be the cause of all these positive anomalies in TEC and LST. This is initial research, and more work is needed to contribute broadly for the earthquake forecasting.

Table of Content

List of Figures

CHAPTER 1

Introduction

1.1 Overview

Massive tectonic plates that make up the surface of the earth have been gently moving over, beneath, and past each other for millions of years, by process of plate tectonics. During this process energies are stored between the plates and these energies build up and try to release from sub surface causing earthquakes. Earthquakes are one of the most dangerous natural disasters and some have even wiped-out whole civilizations (Ambraseys & Douglas, 2004).

Earthquake studies are now not limited to seismologists only, people from various fields like, engineering, town planning, geophysics, and space scientists are studying earthquakes according to their objectives Various techniques are being used to get more and more knowledge of earthquake. In recent years earthquake forecasting has been a hot topic of discussion. The use of warning foreshock data, variations in magnetic fields, seismic tremor, shifting groundwater levels, odd animal behavior, observed periodicity, stress transfer concerns, and other methods have all been investigated as potential prediction methods (Holliday et al., 2005). No reliable method has yet been shown by earthquake prediction research. Even though some claims of accurate earthquake predictions exist, they are scarce, and many of them are associated with questionable circumstances. One of such technique is pre-earthquake ionospheric anomalies analysis.

In recent years the Ionospheric study regarding earthquake is becoming common because total electron content (TEC) in ionosphere has been reported to deviate from normal before an earthquake occurs especially a large magnitude earthquake. The pre-earthquake ionospheric anomaly is an important factor for predicating future earthquakes. Various studies have been done on individual earthquakes with regards to TEC anomalies (Liu et al., 2004). This study uses GPS data to examine changes in ionosphere with regards to TEC for earthquakes that are shallow. Earthquake with magnitude seven or above are our research interest from year 2001 to 2018.

1.2 Ionospheric Anomalies

About 50 to 1000km above surface of the earthquake a neutral gas layer is present, and that layer is called ionosphere since short wave solar radiation produces ionized gases. Ionosphere gives predictable values which are measured using IGS stations installed at various places on earth. In the past, scientists used direct observation and statistics to describe objects or phenomena on earth. We can currently monitor the world from space thanks to the launch of artificial geodetic satellites. These satellite geodetic observations are increasingly concentrating on planetary and lunar investigations. Early in the 1980s, the US Department of Defense developed the Global Positioning System (GPS), an artificial satellite navigation system, for the first time, initially for military use (Kutiev et al,2007). Later, similar satellite systems were produced by other nations as well, including GLONASS by Russia, Galileo by the European Union, and Compass (Beidou) by China (Barrile et al., 2006). The Global Navigation Satellite System (GNSS) is the name of these satellite navigation systems. Although GPS was developed for navigation, it is also beneficial for broad earth observation, such as studying the atmosphere and crustal deformation. Recently, GPS provided a substitute technique for examining the temporal and geographical behavior of the ionosphere (Heki & Ping, 2005). When passing through the ionosphere, the GPS satellites' electromagnetic pulses are delayed. Through the measurement of Total Electron Content (TEC), it is possible to determine the variance in the ionosphere using this time delay. Variance in ionosphere can be due magnetic storms (Ghaffari et al, 2021), space whether conditions, solar activities, and earthquakes (Şentürk & Çepni, 2018). This research is focused on ionospheric anomalies related to earthquake.

1.3 Objectives of the Research

The main purpose of this research is to find ionospheric anomalies before large earthquake (M>7) and shallow earthquake(Depth<50Km), The result of the study will be helpful to predict the anomalous behavior of ionosphere with respect to earthquakes. The research aims are explained as follows,

1. To contribute for the detection of potential ionospheric disturbance due to seismic events.

2. To improve the forecasting of lithosphere atmosphere and ionospheric coupling phenomena to take precaution and minimize their impact on technological infrastructure.

3. To correlate the geomagnetic storm variations with the ionosphere.

1.4 Study Area

This research is done on earthquake from all over the world. Selected earthquakes that fall into our criteria are shown in the Figure 1.1 with red star being epicenters. We have selected data from 2001 to 2018. Among which the earthquakes of Papua New Guinea, China, Russia, Indonesia, Turkey, Costa Rica, Pakistan, and Nepal are included.
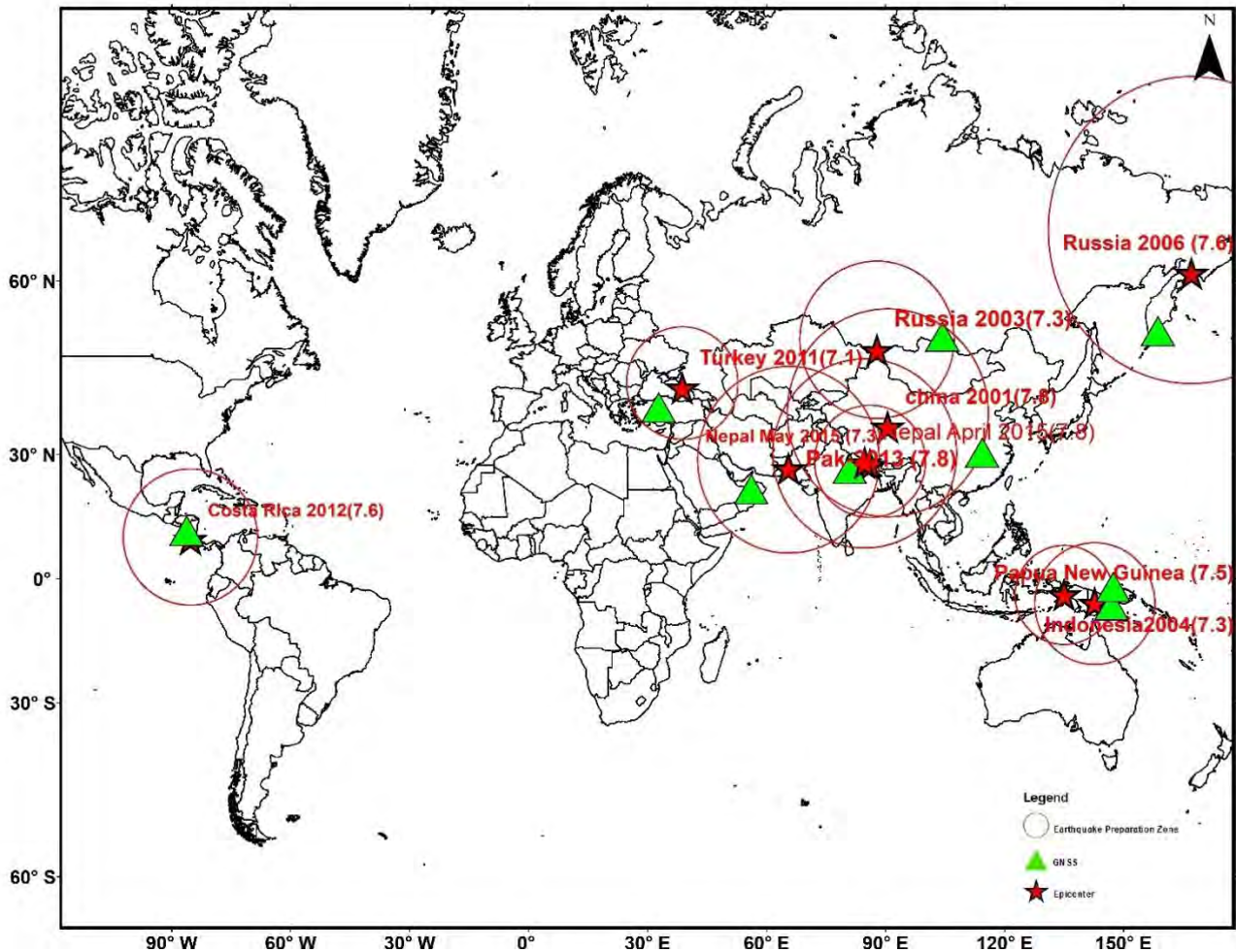
Figure 1.1: Epicenter and IGS station within earthquake presentation zone are shown with red star and green triangle respective for each earthquake.

1.5 Data Sources and Methodology

Data sets used for this research are as following.

1. Earthquake data (Search Earthquake Catalog (usgs.gov)).
2. Magnetic indexes data (https://data.nasa.gov/SpaceScience/OMNIWeb-Plus/)
3. GPS-TEC data (https://cddis.nasa.gov/Data_and_Derived_Products/GNSS/).
4. MODIS data (https://ladsweb.modaps.eosdis.nasa.gov/).

The steps in proposed methodology are as follow.

1. Initially, literature review has been done to thoroughly understand the research and previous works done.
2. Earthquake catalogue is used to filter out the required earthquake; greater or equal to 7 in magnitude and less than 50km.
3. Our focus is on earthquake with epicenter at land. More than 240 earthquakes appeared among which most of them were oceanic earthquake, so we eliminate the earthquakes that are in ocean because GNSS stations are installed in land. To remove the earthquakes that are present in ocean we plotted all the given earthquakes on Google earth pro (https://earth.google.com/web/) and visited single earthquake one by one to filter out land based and oceanic earthquakes.
4. Dobrovolsky's radius calculation for remaining earthquake.
5. Searching for IGS station within the Dobrovolsky's radius. Many earthquakes got eliminated because of unavailability of GNSS station within the earthquake preparation zone and others got eliminated due to unavailability of data on the station at the required time.
6. GNSS-TEC data collection for remaining earthquakes. Downloading 15 days before and 10 days after observation and navigation in RINEX format.
7. VTEC, upper and lower bound calculation.
8. Geomagnetic indexes retrieval and plotting for selected days of the earthquakes.
9. Secondary data (LST) downloading, processing, and analysis.
10. Data analysis, results, recommendation, and Conclusion.

CHAPTER 2

Ionospheric Anomalies and Earthquakes

2.1 Introduction to Ionosphere

The X-rays and extreme ultraviolet energy from the sun, which are the most powerful parts of the solar spectrum, strike the illuminated side of the Earth and cause the formation of the ionosphere. The ionosphere is where incoming energy from the Sun ionizes molecules in the atmosphere, knocking off electrons. It starts at about 48 kilometers above Earth's surface and extends to about 965 kilometers (Forbes et al., 2000).

Due to the high concentration of charged particles, the ionosphere responds to electric and magnetic forces, unlike other parts of the atmosphere. The ionizing beam weakens gradually as it enters the atmosphere, leaving a layer of ionization behind. The magnetic fields of the Earth and the sun both have an influence on charged particles in the ionosphere. Auroras occur here, which are stunning bands of light that occasionally appear close to Earth's poles. They are brought on by the interaction of high-energy solar particles with the atoms in this region of our atmosphere. The free electrons build up in the ionospheric region and interfere with radio signal propagation by adding an extra transmission time delay (Klobuchar,1987).

The size of the delay in trans-ionosphere satellite radio communication is directly proportional to the number of TECs along the line of sight from the satellite to the receiver on the ground and inversely proportional to the square of the frequency (Teunissen et al.,2003). As a result, TEC is a crucial ionosphere parameter and affects how well radio communications, positioning, and navigation applications work.

2.2 Ionosphere and Earthquake

A complex nonlinear dynamic process called an earthquake causes several intricate geophysical and geochemical processes both before and after the occurrence. The seismo-ionospheric phenomenon, which was first described by Moore in 1964 and Davies and Baker in 1965 when examining the anomalous ionospheric disturbance linked to the 1964 Alaska earthquake (Baker et al., 1984). Seismo-ionospheric processes describes

the phenomena of the correlation between earthquakes and ionosphere. Seismo-ionospheric research are becoming popular because a lot of cutting-edge equipment (e.g GNSS) that can track seismo-ionospheric disturbances and seismo-ionospheric plasma perturbations produced by earthquakes both on Earth and in space (Ding et al., 2011). Pre-earthquake and post-earthquake anomalies can be an important factor in describing the effect of earthquake on ionosphere. The ionosphere is reported to show anomalous behavior few days prior to an earthquake. The anomalies vanish few days after the event and do not appear again (Liu et al, 2004).

2.3 Theories Explaining the PEIAs

There are two main theories explaining the phenomenon of how earthquake can cause disturbance in ionosphere. Freund and Sornette in 2007 gave the idea that increase and decreases of TEC in ionosphere occur due to the squeezing of rocks due to tectonic activity or stresses near the epicenter while another seismologist explained it as because of radon gas emission.

It has long been understood by scientists that certain crystals can generate electricity when compressed, a phenomenon known as piezoelectricity. By stressing a piece of granite and observing the resulting electrical current, this phenomenon has been duplicated in the labs as well. Strong strains on rocks along faults can induce piezoelectric phenomena that release free positively charged ions in the days, weeks, and months before to earthquakes. These ions rise upward when discharged into the atmosphere because of the Earth's overall electromagnetic field. These positive ions can move upward in 20 to 30 m/s speed These ions travel till they reach ionosphere (Freund,2011). Influx of solar radiation in earth magnetic field can cause disturbance in ionosphere which have been extensively researched due to their effect on the communication and GPS. Just like solar radiations can cause electric perturbation in ionosphere, positive ions released prior to earthquake can also affect ionosphere causing ionospheric anomalies (Freund & Sornette, 2007).

On the other hand, Pulinets proposed a model relying on Radon gas emission from the active seismic zones in earthquake preparation area. Due to its radioactivity, capacity to move over relatively large distances from its source rocks, and traceability

even at extremely low levels, radon (222Rn), a radiological inert gas, has been recognized as an important trace gas in hydrogeology, earth, and atmosphere studies (Richon et al., 2007). Therefore, studies of radon and its progeny have already been conducted in geothermal fields, sesimo-tectonic studies, active faults, and volcanic processes (Whitehead et al., 1985). In that model, Pulinets brought up the idea that the ionospheric potential above the future earthquake's epicenter may change depending on whether the heating rate of the atmosphere was rising or falling due to constant gas release from the earthquake zone (Pulinets et al., 2003). Both theories are reasonable and one thing we cannot deny is the fact that there exists are relationship between earthquake and ionospheric changes.

It is known that atmospheric waves propagating from the lower atmosphere can also generate ionospheric oscillations in addition to solar activity, the solar flares, and disturbances in the magnetosphere According to studies, these three categories of external sources each contribute roughly the same amount to ionospheric variations (Forbes et al., 2000; Rishbeth, 2006). Currently, typical analyses of pre-earthquake ionospheric disturbances frequently eliminate the impacts of solar and geomagnetic activity.

2.4 Literature Review

A lot of research has been done of ionospheric changes related to earthquakes and ionospheric effects have been thoroughly documented. They contain enormous waves that cover vast distances and are referred to as travelling ionospheric disturbances (TIDs). TIDs are typically caused by storms and weather fronts in the lower atmosphere or by auroral disturbances in the high-latitude ionosphere. The ones noted on March 28, 1964, by ionosondes in Colorado (Davies & Baker, 1965), Alaska, California, and Hawaii (Calais & Minster, 1998), appeared to have originated earlier that day near the huge Alaskan earthquake (M=9.2). As demonstrated by Artru and his colleagues, seismic waves can in fact pair with the atmosphere (Artru et al.,2001).

About 100 ionosondes throughout the world keep hourly records. Although orbiting satellites provide greater reach, their data are constrained by the whims of the earth's orbit. The total ionospheric electron concentration along slant pathways from radio transmitters on Global Positioning System satellites to a terrestrial receiver has recently

been used to discover precursors. This method merits greater adoption due to its outstanding benefits of continuity and extended global reach. Many potential precursor processes for earthquake have been used. Which include the transportation of ions to the ionosphere produced by radon released from the Earth's crust where seismic stress appears to exist (Pulinets et al. 2003; Pulinets & Boyarchuk, 2004) and the transmission of electromagnetic noise or electric fields from seismically stressed areas (Parrot et al., 1993).

In their thorough analysis of one month's data from the European ionosonde network, (Pulinets et al.,2003) conclude that the geographic scales of the presumed precursors are compatible with seismic events. Deeper earthquakes have better antecedents than shallow earthquakes (Silina et al.,2001). In Taiwanese ionospheric data spanning 1994–1999 (Chen et al.,2004) discovered a very positive association between 170 earthquakes with Richter magnitudes greater than five and 307 putative precursors, with an arbitrary lead period of five days.

Today's modern Global Positioning System (GPS) can compute atmospheric delays, that can be used to track atmospheric and ionospheric disruptions (Jin et al., 2004; Catherine et al., 2017) of the most crucial methods to investigate and comprehend the connection and coupling of the solid Earth and the ionosphere is through seismic ionospheric disturbance (SID). GPS total electron content (TEC) can be used to track the seismically induced ionospheric anomalies, even if it is still very difficult to grasp the mechanism and electrodynamic-atmospheric interactions in the various layers of the Earth (Rolland et al., 2013). Contrasting with conventional ionospheric checking methods, for instance, random dissipating radars and ionosondes, GPS can get close ongoing ionospheric TEC with high accuracy and high transient goal as well as every single climate perception, which has been broadly used to screen seismic ionospheric anomalies and study its variety qualities since 1990s (Calais & Minster, 1995). Throughout the course of recent years, broad exploration has been directed on PEIAs (Pulinets & Boyarchuk, 2004; Rishbeth, 2006; Zhao et al., 2008; Xu et al., 2013; Tariq et al., 2019). As indicated by measurable investigations, ionized layer unsettling influences brought about by seismic action can be noticed days to minutes before the approaching serious quake.

Many questions remain unanswered regarding the origin of these anomalies near the epicenter prior to the EQs, but some studies have found a strong correlation between

the incidence of EQs and ionospheric fluctuation. For instance, from 1998 to 2014 research done by Shah and Jin, showed positive GPS–TEC anomalies five days prior to M > 5.0 EQs. Positive TEC anomalies exceed the number of negative TEC anomalies for all earthquakes. This shows that large magnitude EQs often occur after positive TEC anomalies (Shah & Jin,2015).

Similarly, in 2004 Liu and his colleagues analyzed the statistical significance of GPS-TEC data for earthquake that had magnitude greater than 6 in Taiwan area in time span from 1999 to 2002 during quite magnetic conditions. Their study concluded that 1-5 day prior to an earthquake, decreases in TEC happen leading to ionospheric anomaly (Liu et al., 2004). Same kind of research was done by Le and his fellows, their research shows a positive correlation of earthquake occurrence and TEC anomalies 1-21 days prior to an earthquake having magnitude 7 and depth of 20 km. The reason for ionospheric anomalies is explain through two phenomena. According to (Freund & Sornette, 2007), tectonic activity or stresses close to the epicenter squeeze the rocks, causing changes in TEC in the ionosphere. Pulinets, on the other hand, put forth a model that relied on Radon gas emission from the seismically active zones of the earthquake preparation zone.

CHAPTER 3

Seismotectonic of the Study Area

3.1 Overview of the Earthquakes

Ten major earthquakes have been taken for the research from 2001 to 2018. Table 3.1 summarizes detailed information on these earthquakes, where Mw, occurrence date, geographic longitude, geographic latitude, magnitude, depth and IGS station from which data has been collected, are taken from the United States Geological Survey catalog. These earthquakes have been selected after going through a long process of data filtering at various steps mentioned in chapter 2.

Table 3.1: Details of selected earthquakes

Serial Number	Date	Latitude	Longitude Degree	Magnitude Degree	Depth(km)	Region	GNSS Station
1	11/14/2001	35.946	90.541	7.8	33	China	WUH
2	9/27/2003	50.038	87.813	7.3	10	Russia	IRKJ
3	2/7/2004	-4.003	135.023	7.3	16	Indonesia	LAE
4	4/20/2006	60.949	167.089	7.6	22	Russia	PETS
5	10/23/2011	38.721	43.508	7.1	18	Turkey	ANK
6	9/5/2012	10.085	-85.315	7.6	35	Costa Rica	MANA
7	9/24/2013	26.951	65.5009	7.7	35	Pakistan	YIBL
8	4/25/2015	28.2305	84.7314	7.8	15	Nepal	LCK
9	5/12/2015	27.8087	86.0655	7.3	8.22	Nepal	LHAZ
10	2/25/2018	-6.0699	142.7536	7.5	25.21	PNG	PNGM

3.1 November 14,2001 China

A severe quake with a magnitude of 7.8 struck the Kokoxili region in the north-west of Qinghai, China, on November 14, 2001. This earthquake jolted a sparsely populated territory on the northern edge of the Tibetan Plateau, even though 1,000 km away from the epicenter it was felt. The earthquake occurred on the Kunlun fault, a left-lateral, strike-slip fault on Tibet's eastward expansion (Klinger et al, 2005).

The Tibetan plate is also affected from Indian and Eurasian plate collision. The Kunlun Fault is a strike-slip fault on the Tibetan plate that has the major effect on the earthquake of 2001 in China because of the Indian-Eurasian collision (Xu & Chen,2005). Figure 3.1 represents Geographical Location of the selected earthquake on the globe along with GPS station within earthquake preparation zone.

Figure 3.1: The geographic locations of the GPS stations within earthquake preparation zones, and EQ epicenters for the China earthquake of November 14, 2001.

3.2 September 27, 2003, Russia

On September 27, 2003, a major earthquake with a magnitude of 7.3 took place in the southern part of the Altai Republic. The jolt was felt across a sizable portion of Russia. Landslides, rock falls, flooding, as well as the destruction of homes and other lowland buildings, were all brought on by the earthquake. Several thousand aftershocks were caused by the 2003 catastrophe over the years (Emanov et al, 2021).

Studying the tectonic setting of the Gorny Altai earthquake source has made it possible to trace the main seismically active areas of the Mongolian and Gobi Altai, where earthquakes with a magnitude M > 7.0 frequently occurred (Drachev et al, 2010). Figure 3.2 represents Geographical Location of the selected earthquake on the globe along with GPS station within earthquake preparation zone.

Figure 3.2: The geographic locations of the GPS stations within earthquake preparation zones, and EQ epicenters for the Russian earthquake of September 27, 2003, earthquake of Russia.

3.3 February 7, 2004, Indonesia

A lot of small earthquakes have been occurring in the region a week prior to the major earthquake, this one was disastrous. Which not only caused damaged to building but lives as well. At least 37 people were killed and were 682 injured, and over 2,600 buildings were damaged or destroyed due to the earthquake (Madlazim, 2012).

Indonesia frequently experiences earthquakes and volcanic eruptions because of its placement on the Pacific "Ring of Fire." Where tectonic plates collide, the Ring of Fire is a region of intense seismic activity that stretches from Japan through Southeast Asia and across the Pacific Ocean (Hall,2009). Figure 3.3 represents Geographical Location of the selected earthquake on the globe along with GPS station within earthquake preparation zone.

Figure 3.3: The geographic locations of the GPS stations within earthquake preparation zones, and EQ epicenters for the Indonesian earthquake of February 7, 2004

3.4 April 20,2006, Russia

On April 20,2006 an earthquake jolted northeastern Russia in a densely populated are The tectonics of this area is difficult to understand how the plates in northeastern Asia and northwest North America interact. This region's sedimentary basins were formed 160 million years ago because of powerful magma that penetrated the crust; hence leading to volcanism. The boundaries between accreted island arcs are usually formed by large faults that have the potential to reactivate and cause earthquakes. Because there are so many of them and they were all produced throughout the accretion process, it might be difficult to determine which, if any, of these old faults burst to generate the Koryakia earthquake. Figure 3.4 represents Geographical Location of the selected earthquake on the globe along with GPS station within earthquake preparation zone.

Figure 3.4: The geographic locations of the GPS stations within earthquake preparation zones, and EQ epicenters for the Russian earthquake of April 20, 2006.

3.5 October 23, 2011, Turkey

Eastern Turkey's Van Province experienced a Mw 7.1 earthquake on Sunday, October 23rd, 2011. During the earthquake, 604 people died. The hardest-hit town was Erciş, which has a population of 77,000 (GOVP, 2011). More than 190 buildings were affected, counting casualties greater than 600 (Tapan et al., 2013). The interplay of the Arabian and Eurasian tectonic plates has created a complex seismic environment in the area surrounding Van. Along with northeast-southwest left-lateral and northwest-southeast right-lateral translational fault zones, the region also features east-west thrust fault zones. The main shock occurred on a WSW-ENE reversing fault with a north-dipping fault plane. Figure 3.5 represents Geographical Location of the selected earthquake on the globe along with GPS station within earthquake preparation zone.
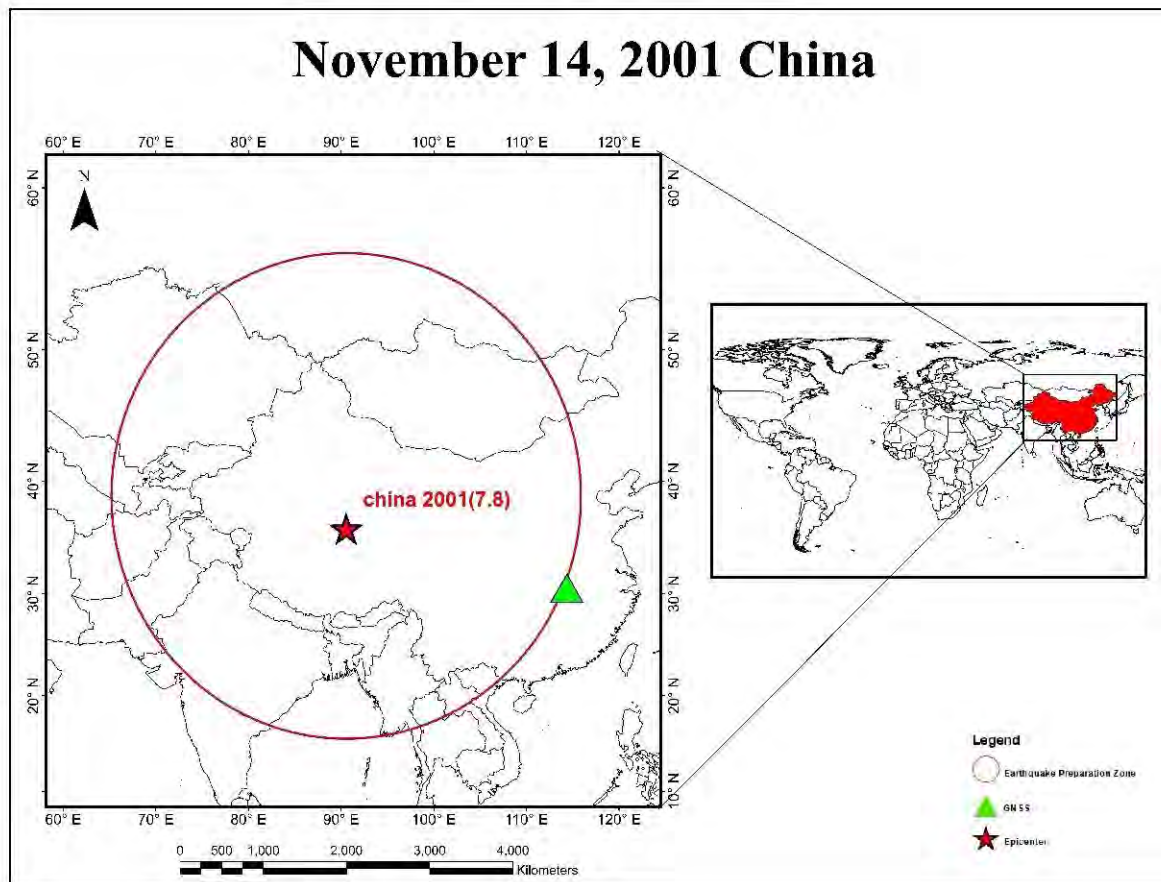

Figure3.5: The geographic locations of the GPS stations within earthquake preparation zones, and EQ epicenters for the Turkey earthquake of October 23,2011

3.6 September 5, 2012, Costa Rica

An inter-plate thrust event with a moment magnitude (Mw) of 7.6 occurred beneath the Nicoya Peninsula on September 5, 2012, which caused highest damaged buildings of the area. Fortunately, very few numbers of causalities were reported in the event

The Cocos Plate subducts beneath the Caribbean Plate along the Middle America Trench (northeasterly direction) at a pace of 8.5 cm per year (Liu et al., 2015). Strong earthquakes commonly occur in the Nicoya region of northwest Costa Rica because of this rapid convergence rate. Figure 3.6 represents Geographical Location of the selected earthquake on the globe along with GPS station within earthquake preparation zone.
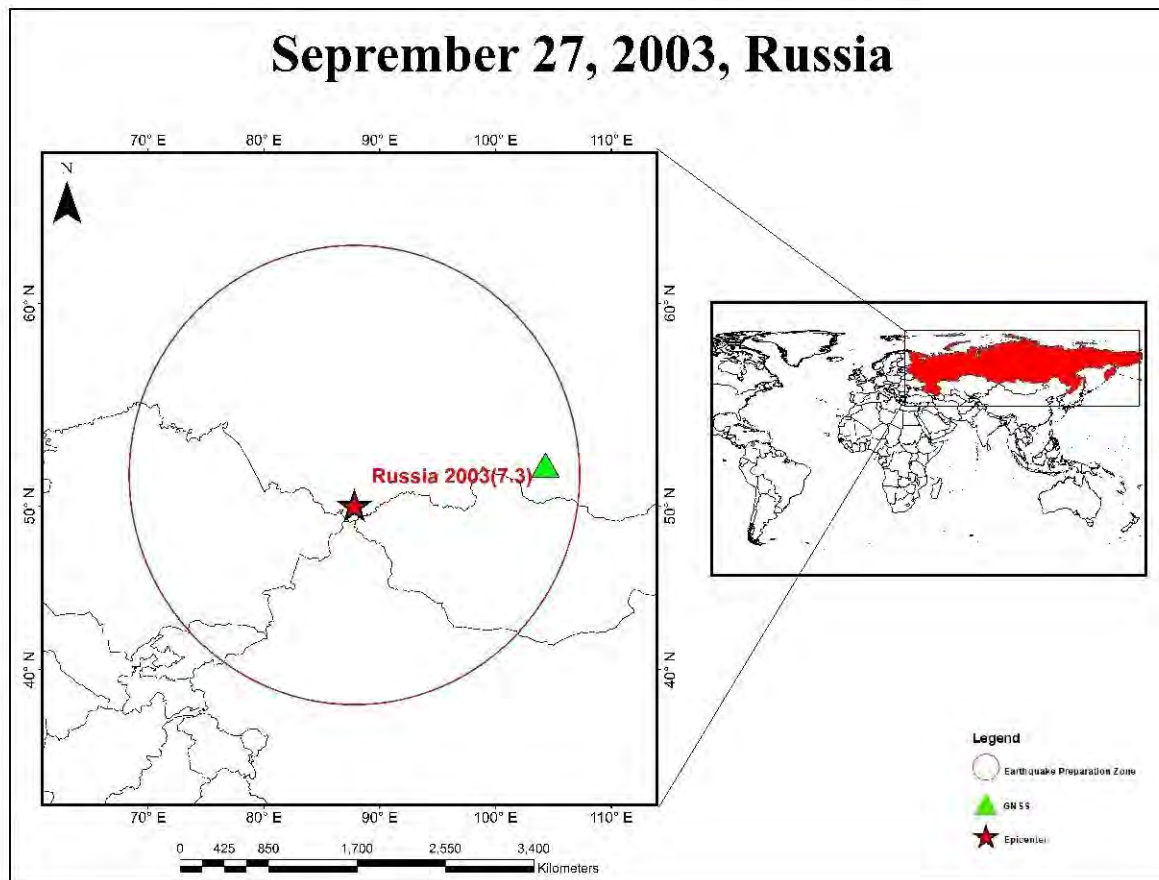

Figure 3.6: The geographic locations of the GPS stations within earthquake preparation zones, and EQ epicenters for the Costa Rica earthquake of September 5, 2012.

3.7 September 24, 2013, Pakistan

September 24, 2013, is marked as one of the big earthquakes that struck southern Pakistan. Bella is an area in Baluchistan province where a magnitude 7.7 earthquake cause destruction. Since the area is less populated number of casualties were reported as 825 and many more were injured. Oblique strike-slip motion at shallow earth's crust depths led to the M 7.7 earthquake. The incident took place in the region where the Arabian Plate was being subducted under the Eurasia Plate and the India Plate was colliding with the Eurasia Plate in the north. The area is tectonically active but fortunately from past four decades no major destructive earthquake has been experienced (Muhammad et al, 2013). Figure 3.7 represents Geographical Location of the selected earthquake on the globe along with GPS station within earthquake preparation zone.
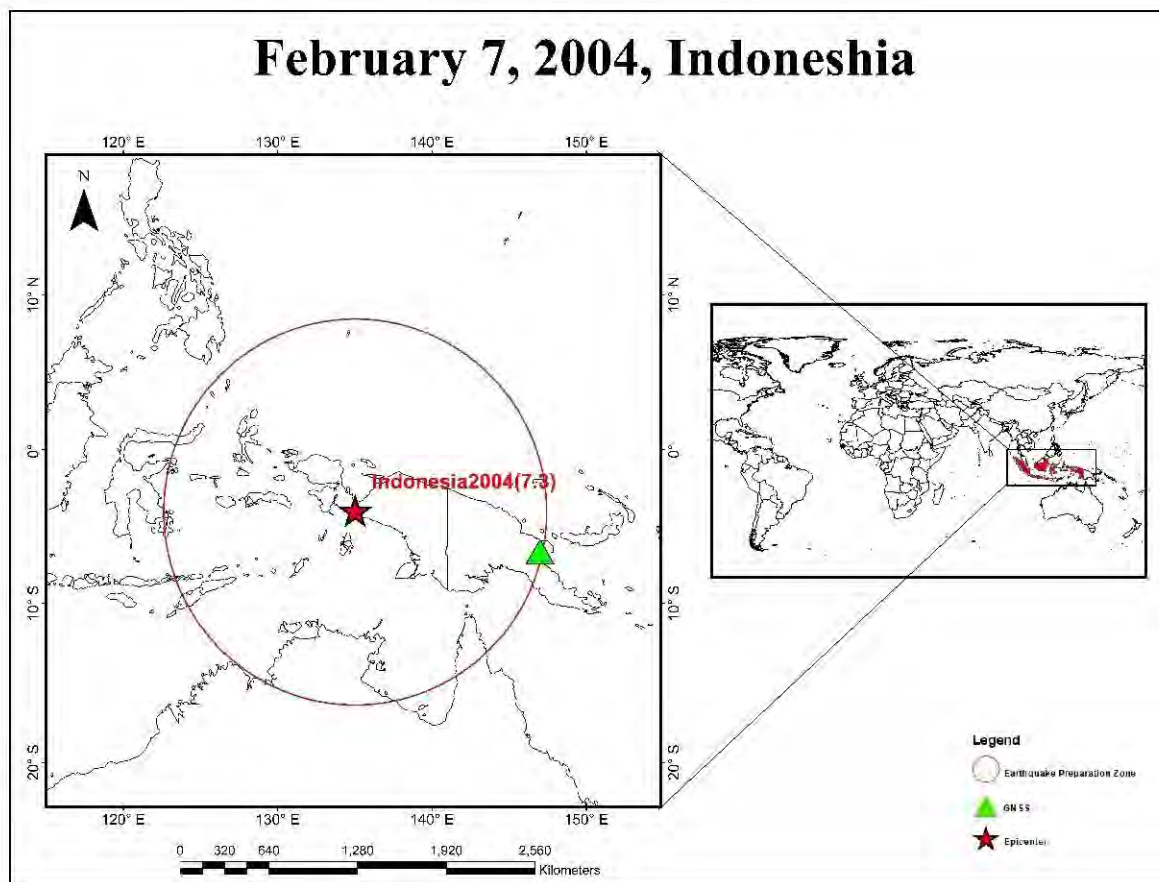

Figure3.7: The geographic locations of the GPS stations within earthquake preparation zones, and EQ epicenters for the Pakistan earthquake of September 24, 2013.

3.8 April 25, 2015, Nepal

The 2015 Nepal earthquake, also known as the Gorkha earthquake, was a powerful quake that occurred on April 25, 2015. Its focus was 15 km underground, and its epicenter was roughly 77 km northwest of Kathmandu. Within a day of the first quake, the area had two prominent aftershocks with magnitudes of 6.6 and 6.7, and several smaller aftershocks followed in the following days. About 9000 people were killed and thousands were injured. The thrust faulting that caused the earthquake and its aftershocks occurred in the Indus-Yarlung suture zone, a thin east-west region that roughly spans the extent of the Himalayan peaks. The earthquake reduced compressional pressure between the Indian component of the Indo-Australian Plate, which subducts under the e Eurasian tectonic plate. Figure 3.8 represents Geographical Location of the selected earthquake on the globe along with GPS station within earthquake preparation zone.
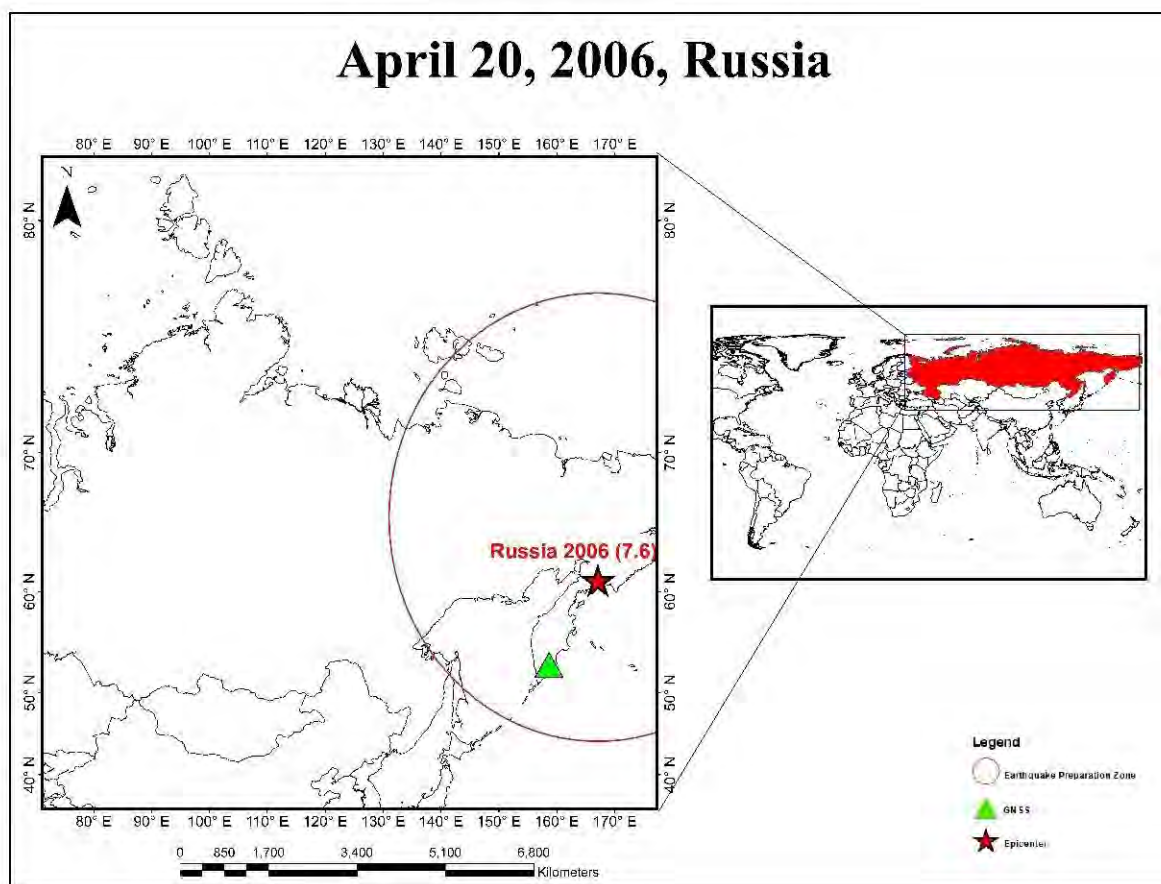

Figure 3.8: The geographic locations of the GPS stations within earthquake preparation zones, and EQ epicenters for the Nepal earthquake of April 24, 2015.

3.9 May 12, 2015, Nepal

A magnitude-7.3 aftershock that occurred on May 12 about 76 km east-northeast of Kathmandu, that killed over 100 people and injured 1,900 more. It triggered landslides which led to killing of local people. The Initial estimates of the damage were between $5 billion and $10 billion. The earthquake also caused an avalanche on Mount Everest, which left hundreds of climbers stranded at Everest Base Camp and other camps higher up the mountain. Indo-Australian plate subducts under Eurasian plate which leads to uplifting of Himalayan ranges. The rate of subduction in Himalayas is high approximately 4-5 cm each year because of this activity height of Himalayan peaks increases 1cm per annum. Figure 3.9 represents Geographical Location of the selected earthquake on the globe along with GPS station within earthquake preparation zone.
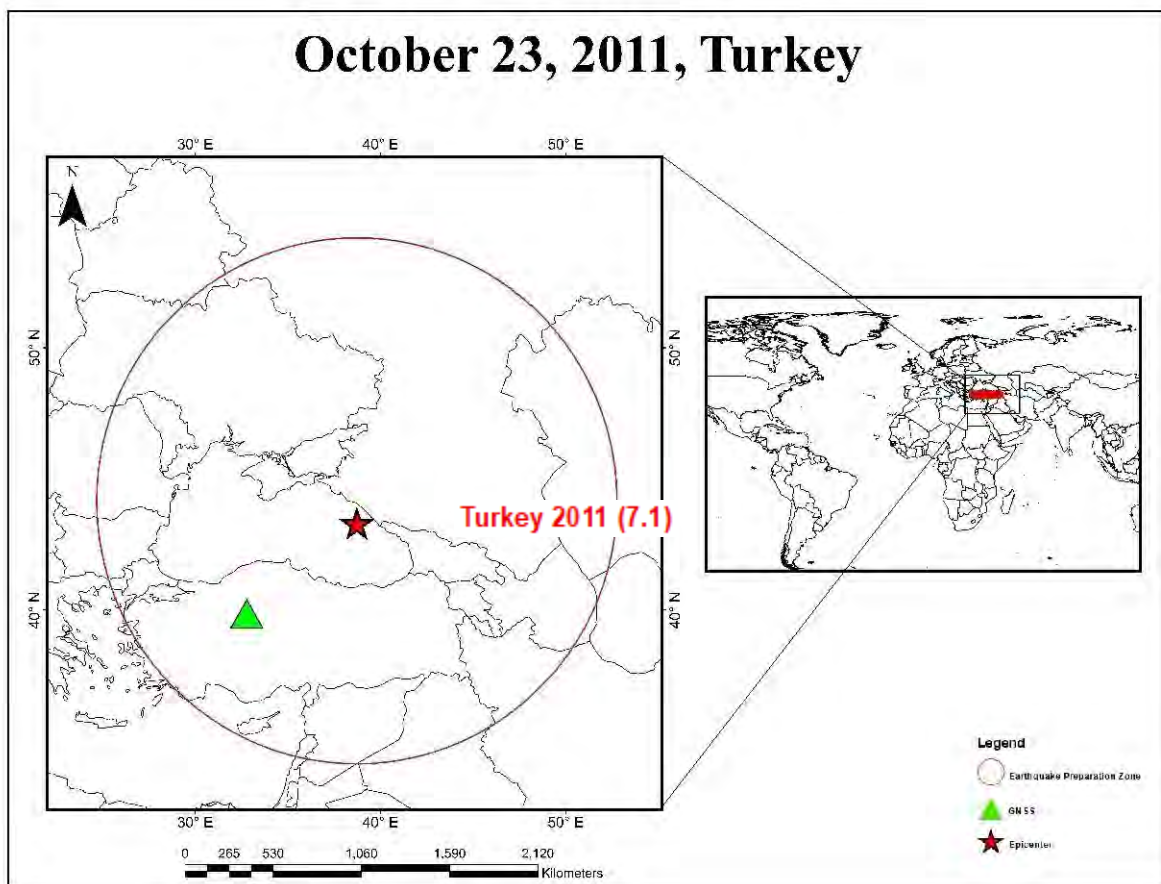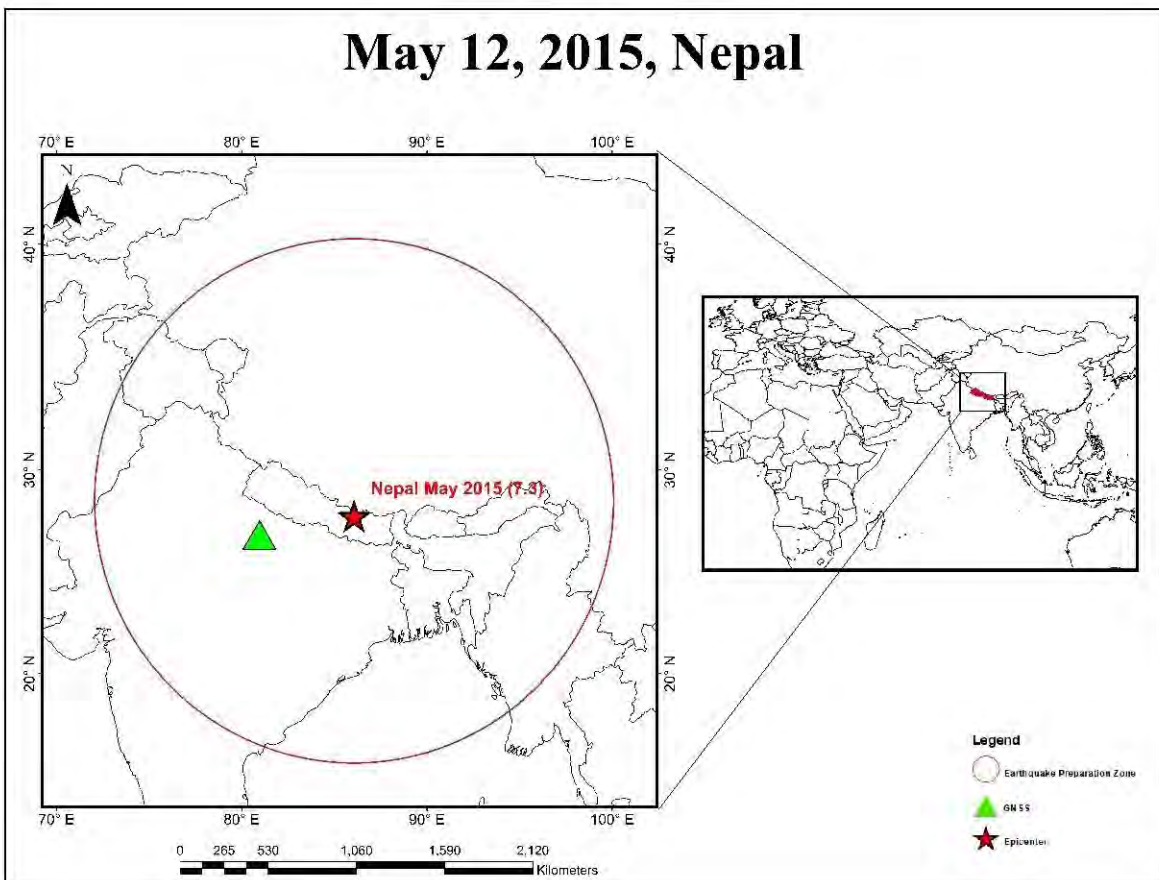

Figure 3.9: The geographic locations of the GPS stations within earthquake preparation zones, and EQ epicenters for the Nepal earthquake of May 2012, 2015.

3.10 February 25, 2018 Papua New Guinea

A magnitude 7.5 earthquake hit Papua New Guinea on February 25, 2018. It triggered landslides in hilly areas and led to burial of people and properties including crops and other resources (Wang et al, 2020).

The huge earthquake occurred due to thrust faulting at shallow a depth. The Australia plate is colliding with the Pacific plate at the epicenter of this earthquake and is moving toward the east-northeast. The large-scale convergence of these two major plates and the intricate interactions of several related microplates, are often linked to earthquakes in this vicinity (Tanyaş et al., 2022). Figure 3.10 represents Geographical Location of the selected earthquake on the globe along with GPS station within earthquake preparation zone.
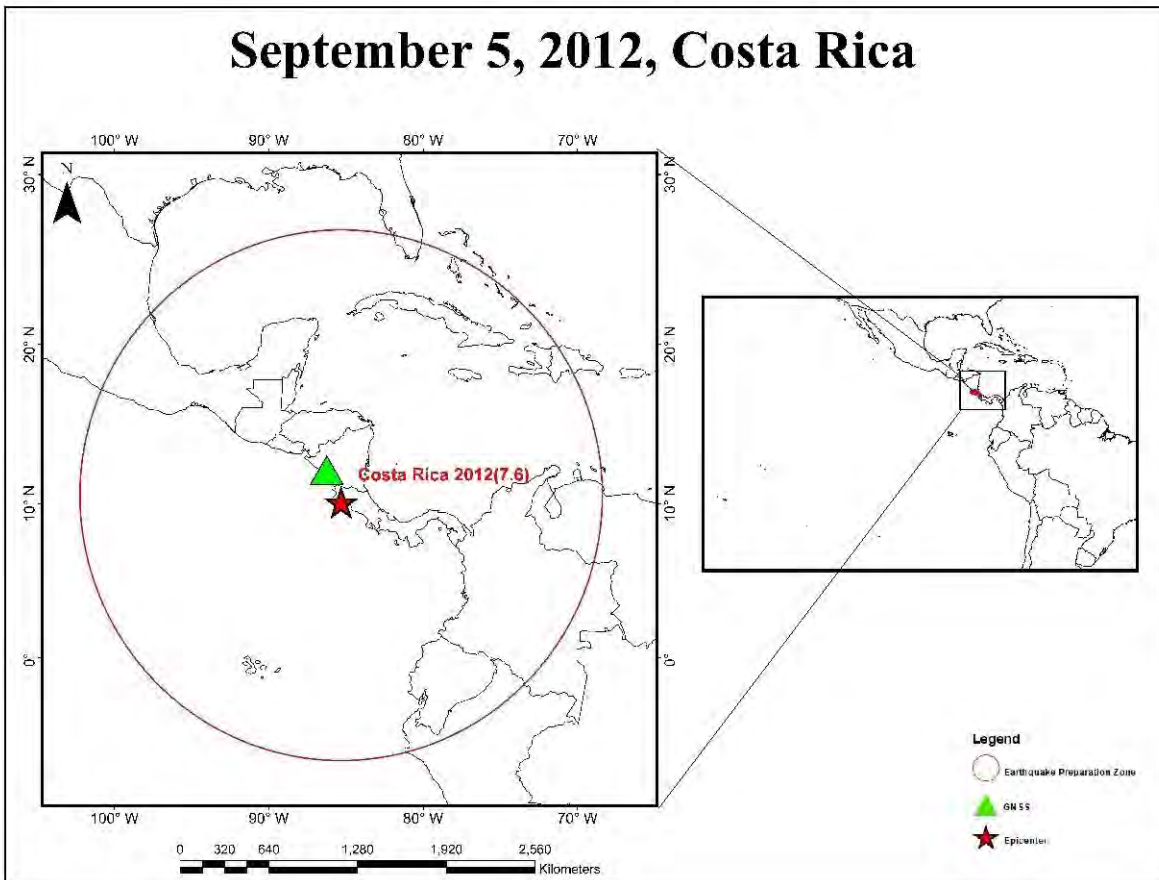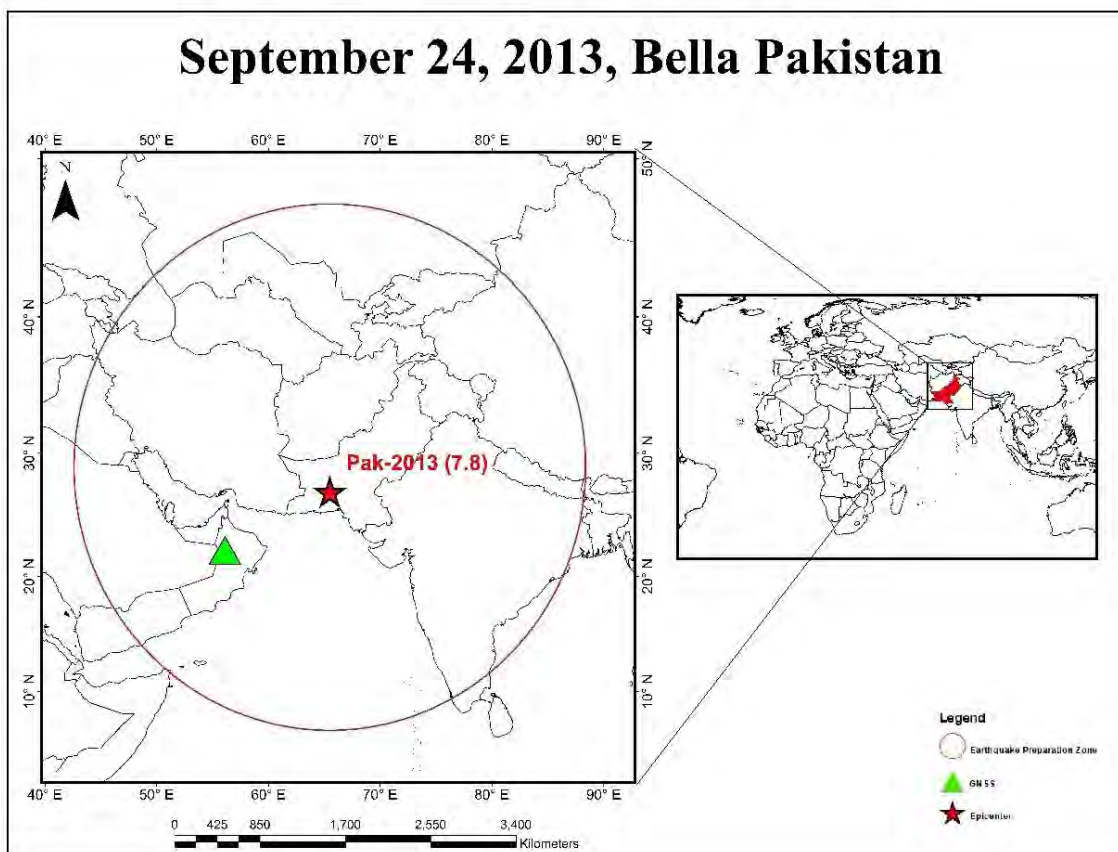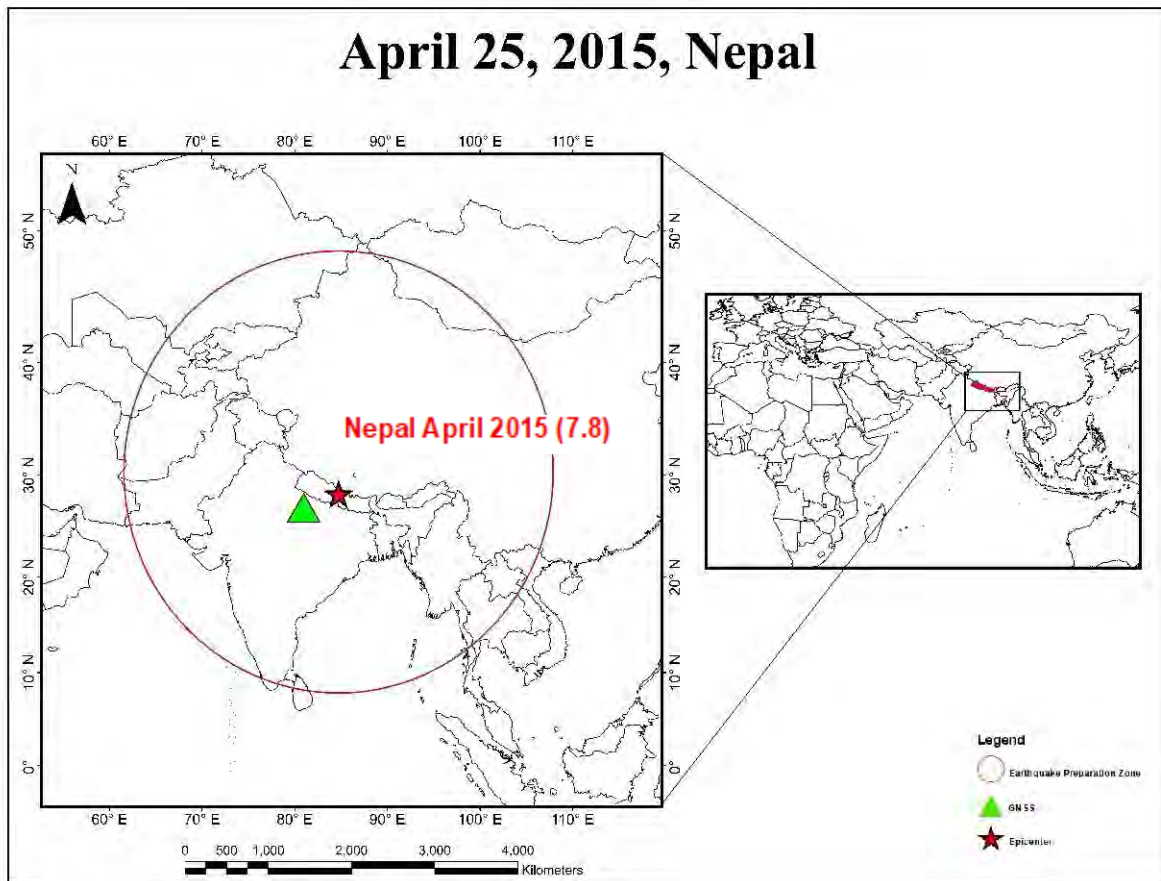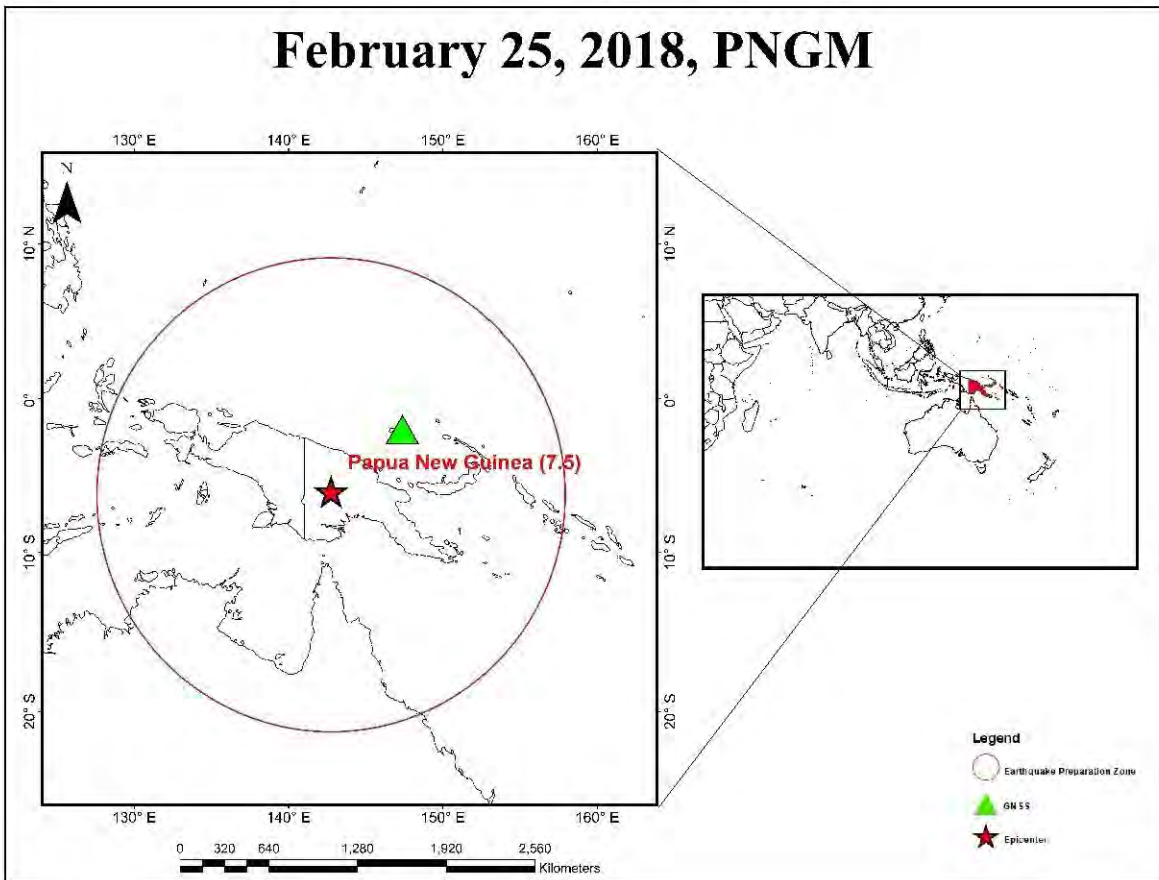

Figure 3.10: The geographic locations of the GPS stations within earthquake preparation zones, and EQ epicenters for the Papua New Guinea earthquake of February 25, 2018.

CHAPTER 4

Data Processing and Methodology

4.1 Overview

Total electron content is the main factor that can help in finding out the ionospheric anomalies before an earthquake. Various satellites with advanced technology can monitor and measure the TEC of the ionosphere. With the help of this data, we can see the disturbance in the ionosphere whether from external or internal factor which includes solar flares, magnetic storms, volcanism, lightning, and earthquakes. A lot of research in various areas of the world has been done in this regard to see the effect of the earthquake on the ionosphere. Global navigation system stations (GNSS) are installed around the world that can monitor ionospheric anomalies.

This research used available GNSS data from all over the world to observe the ionospheric anomalies for earthquakes that are greater than 7 in magnitude and less than 50 km in depth from 2001 to 2018.

4.2 Data sources and collection

4.2.1 Earthquake Data

USGS earthquake catalog data has been used to find out the earthquakes data (Search Earthquake Catalog (usgs.gov)). An earthquake with a magnitude equal to or greater than 7 with depth less than 50 km has been selected for the research. More than 240 earthquakes appeared among which most of them were oceanic earthquake. Elimination of the earthquakes that are in ocean has been done because GNSS stations are installed in land. To remove the earthquakes that are present in ocean the data is plotted on Google earth pro (https://earth.google.com/web/) and visited single earthquake one by one to see whether it is located on land or ocean. After going through this extensive filtering process, 10 earthquakes are used in the research.

4.2.2 GPS-TEC Data

Once the earthquakes have been filtered out based on locations, Dobrovolsky's radius is calculated and GNSS stations within the radius are scanned to get the required data. Many earthquakes got eliminated because of unavailability of GNSS station within the earthquake preparation zone and others got eliminated due to unavailability of data on the station at the required time. After this extensive work 10 earthquakes which have GNSS data available are processed further. For each 10 earthquakes the data is navigation and observation data are downloaded for 15 days before and 10 days after the event from(https://cddis.nasa.gov/Data_and_Derived_Products/GNSS/). These files are processed to get required VTEC data which is further explained in data processing chapter

4.2.3 Geomagnetic Indices

A geomagnetic storm is a significant disruption of the magnetosphere that happens when energy from the solar radiation is exchanged very effectively into the space environment around Earth. These storms are the result of fluctuations in the solar wind, which significantly alter the currents, plasmas, and fields in the magnetosphere of the Earth. A coronal mass ejection (CMEs), —a powerful burst of solar wind or where roughly one billion tons of solar plasma with an embedded magnetic field reach Earth. This burst of solar wind causes the Earth's magnetic field's outer region to oscillate in a complex way. This causes associated electric currents to flow in the vicinity of Earth, and that in turn causes more magnetic field changes, resulting in what is known as a "magnetic storm. A high-speed solar wind stream is another solar wind disturbance that fosters the development of geomagnetic storms. Another reason for magnetic storms to happens is on occasion, where the magnetic fields of the Sun and Earth are in direct contact. It is not usual for there to be a direct magnetic interaction. When it happens, charged particles moving along magnetic field lines can easily reach the magnetosphere, produce currents, and lead to time-dependent variations in the magnetic field.

It is necessary to confirm the geomagnetic indices for the space weather environment to confirm the EQs-induced anomalies in the TEC data. Various parameters are used to identify disturbed days among which Kp, Dst, and F10.7 index are the most common in-

dexes which helps us study geomagnetic conditions of the day. To achieve this, the magnetic indexes are downloaded from (https://data.nasa.gov/SpaceScience/OMNIWebPlus/). Studying geomagnetic conditions is very important for our study purpose, if these are not taken into consideration, it can affect our study drastically.

Kp Index

Geomagnetic storm magnitude is measured using the K-Index. Kp is a good way to detect changes in the Earth's magnetic field. The Kp-index measures the geomagnetic activity globally every three hours using data from magnetometers installed on the ground. The Kp-index has a range of 0 to 9, with 0 denoting very little geomagnetic activity and 9 denoting intense geomagnetic storming.

Dst Index

Likewise, Geomagnetic storm strength and duration are examined using the Disturbance Storm Time (Dst) index. Dst is a unit used to describe how much the magnetosphere ring current has increased while the horizontal component of the Earth's magnetic field has decreased near the magnetic equator. A high level of geomagnetic activity is indicated by readings below -50 nanoteslas (nT).

F10.7 Index

Furthermore, solar radio flux at a wavelength of 10.7 cm (2800 MHz) is a very good measure of solar activity. It is one of the oldest records of solar activity and is frequently referred to as the F10.7 index. Traditionally, this indicator has served as a stand-in for the solar output at wavelengths that cause photoionization in the earth's ionosphere in ionospheric models.

4.2.4 MODIS Data

Two NASA spacecraft, Terra and Aqua, which were launched in December 1999 and May 2002, respectively, are equipped with MODIS equipment. The data from the Aqua and Terra satellites have a temporal resolution of twice daily because they are both near-polar 160 orbit spacecraft with a flight height of roughly 705 km in sun-synchronous

orbit. The morning star, or Terra satellite, crosses the equator from north to south at between 10:30 am and 10:30 pm local solar time. The Aqua satellite, on the other hand, is referred to as the afternoon satellite since it travels through the equator at 1:30 am and 1:30 pm in the opposite direction from south to north (Vancutsem et al., 2010).

For many scientific domains, it is a crucial sensor that monitors the ocean, atmosphere, land, and ice. In the electromagnetic spectrum, MODIS records 36 distinct spectral bands with wavelengths ranging from 0.4 m to 14.4 m. In a grid of 1200 by 1200 km, the MOD11A1 product offers daily per-pixel LST and Emissivity (LST&E) with a spatial resolution of 1 km (Wan & Li, 1997). LST data accuracy is approximately 1 K. Modis data is retrieved from (https://ladsweb.modaps.eosdis.nasa.gov/)

4.3 Data Processing

Studies conducted by western scientists showed that changes in the Earth's crust, including deformations, variations in seismic wave velocity, the emission of gases from the Earth's crust, and changes in crustal electric conductivity are visible not only at the epicenter of an earthquake, but also in the zone that extends an order of magnitude beyond the source dimensions (Soloviev et al., 2014). This allowed scientists to create the dilatation theory, which describes how the Earth's crust was deformed, fractured, and formed a primary fault in the area known as the earthquake preparation zone (Mjachkin et al., 1975). According to Dobrovolsky's et al. (1979), the elastic deformation of the Earth's crust at a level of 10-8 can be represented as follows:

$$\mathbf{R=10^{0.43M}}\, \mathrm{Km} \dots\dots\dots\dots\dots\dots\dots\dots\dots\dots\dots\dots\dots\dots\dots\dots\dots\dots \quad (1)$$

R is the radius of the preparation zone and M is the magnitude of the earthquake. The radii for all earthquakes above 7 magnitudes have been calculated. All GNSS stations within the earthquake preparation zone are scanned to collect available data. Because the GNSS signals travel through the ionosphere carrying indicators of the dynamic medium, they are a great instrument for monitoring ionospheric fluctuations (Tariq et al.,2019).The observed GPS-TEC data are obtained for all the earthquake, to get a quantitative information of Pre earthquake anomalies for earthquake forecast. Slant TEC is number of electrons in path of the signal that is one square meter. Its unit is TECU that is

equal to 10^{16} electron/m². Slant TEC can be calculated with the help of following equation from dual frequency GPS receiver (Jin et al., 2014).

$$STEC= \frac{f_1^2 f_2^2}{40.28(f_1^2 - f_2^2)}(L_1 - L_2 + \lambda_1(N_1 - b_1)\text{-} \lambda_2(N_2 + b_2)+\in) \text{---------------------- (2)}$$

Here f1 and f2 are the carrier phase frequency of the signal, L is the carrier phase monitoring of the GPS signal delay path, and is the wavelength of the GPS signals, N is the beam path anomaly, while b and d are the carrier phase and over-range instrumental biases for the derived signal, and ε is a random residual of the signal. STEC can be converted to VTEC with the help of a mapping function (Klobuchar, 1987).

$$VTEC = STEC\cos \times (\text{arcsine} (\frac{Rsinz}{R+H})) \dots\dots\dots\dots\dots\dots\dots\dots\dots\dots\dots\dots \text{(3)}$$

R, Z, and H are the radius of the earth, the satellite elevation angle for the observation point, and Z is the height of the ionosphere above the surface of the earth respectively (Heki & Enomoto, 2013).

Once we have VTEC data we can compute the required deviation of VTEC from normal. We determine the first (or lower) and third (or upper) quartiles, designated by LQ and UQ, respectively, to provide the information on the deviation. We also find the median of the data along with finding the difference between the observed value on the twenty-fifth day and the computed median by computing the median of each subsequent set of 25-day values. It is important to note that the values of M and LQ or UQ under the assumption of a normal distribution with mean and standard deviation r for the VTEC are 1.34r, respectively (Klotz and Johnson, 1983). The upper and lower bounds are found with the help of the following formula.

$$LB = M\text{-}1.5(M\text{-}LQ) \dots\dots\dots\dots\dots\dots\dots\dots. \text{(4)}$$

$$UB = M + 1.5(UQ\text{-}M) \dots\dots\dots\dots\dots\dots\dots. \text{(5)}$$

Any signal that deviates from either the lower or upper bound can be considered as an anomaly based on the calculations with a confidence level of 65-70% (Neter et al., 1988).
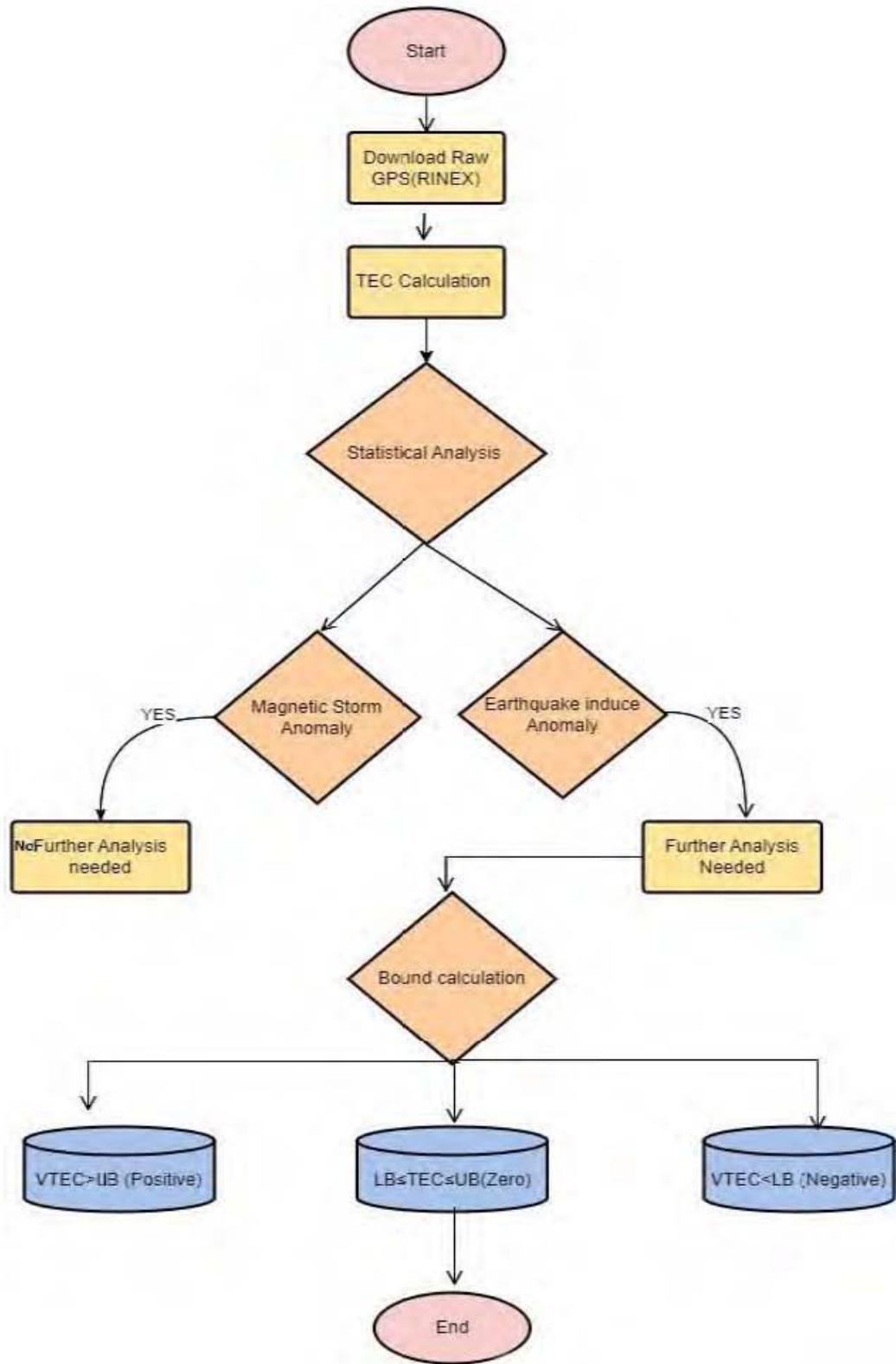
Figure 4.1 Generalized workflow for utilizing GPS TEC data to analyses Pre-earthquake ionospheric anomalies.

CHAPTER 5

Data Analysis and Results

5.1 Overview

This study explored pre-earthquake VTEC changes for earthquake with magnitude greater than seven or equal to7. the study has been carried out on VTEC time series fifteen day before and ten days after an earthquake using GNSS station data within the radius of the earthquake preparation zone. Based on availability of GNSS station near to epicenter, 10 shallow depth earthquakes are selected (>50km). The ionospheric anomalies are not always related to earthquakes, but Continuous observation of GPS satellites gives indication of anomalies few days before main shock that can be related to pre-seismic ionospheric anomalies.

5.2 Ionospheric VTEC variations Analysis

VTEC, lower bound, and upper bound are plotted against days of the years for 26 days including 15 days before and 10 days after the event. The VTEC and dTEC time series, which are obtained from the observations of the Geostationary satellites, show that these anomalies are remarkably consistent. It is important to check for space weather conditions before analyzing the anomalies, which have been studied using geomagnetic indices including Kp, Dst, and F10.7 values. With the help of these geomagnetic indices, differentiation between quiet and disturbed days has been done. For each figure explained below, top 3 panels give information of space weather conditions while bottom two gives information about the temporal VTEC estimation. The earthquake days are indicated by the vertical dashed line. The rectangular box throughout the figure shows the simultaneous occurrence of anomalies during the selected period. Let's see each earthquake in detail.

5.2.1 November 14, 2001, China

November 14, 2001, earthquake of China has been plotted for the specific 26 days (15 days before the event and 10 days after the event) from 303 to 327 days of a year, with 318th day being the event day. The Geomagnetic storm starts at day 309 and gains maximum amplitude at day 310 and gradually descends afterward. It is found that both the dTEC and Temporal VTEC plots simultaneously reveal strong anomalies on two to four days before the earthquake, that is highlighted with blue rectangle in the Figure 5.1 There is enhancement in VTEC two days before the earthquake, which is further validate by dTEC with 20 TECU above Upper bound. Likewise, day 314 and 315 also shows five to six TECU enhancements.

Figure 5.1:Geomagnetic storms indices (a, b, & c) are presented in top 3 panels and bottom 2 panels are representing Temporal VTEC with UB/LB and dTEC of November 14, 2001, China. Solid dashed line marks earthquake day while blue box represents PEIA days.

5.2.2 September 27, 2003, Russia

September 27, 2003, earthquake's data of GPS-TEC and geomagnetic indices along with deviation have been plotted for 26 days which includes 15 days before the event, the event day, and 10 days after the event from 255 to 280 day of the year (2003). Graphical representation of all the parameters is shown in Figure 5.2.

The Geomagnetic storm starts at day 258 and gradually descends to normal conditions at 264th day. Three and six days prior to the earthquake an enhancement can be seen in Figure 5.2 which shows 35 TECU and 20 TECU above upper bound, respectively. These can be a good precursor for earthquake forecasting.

Figure 5.2: Geomagnetic storms indices (a, b, & c) are presented in top 3 panels and bottom 2 panels are representing Temporal VTEC with UB/LB and dTEC of September 27, 2003, Russia. Solid dashed line marks earthquake day while blue box represents PEIA days.

5.2.3 February 7, 2004, Indonesia

Observed VTEC for 26 days is plotted along the calculated upper and lower bound to examine TEC anomalies related to the February 7, 2004, earthquake of Indonesia. Geomagnetic storms are very high at day 23 and gradually descends towards day 27, likewise another storm can be seen at day 42 in Figure5.3. VTEC anomaly at day 31 is observed which is 7 days prior to the main event and it is approximately 12 TECU above upper bound and it can be ionospheric anomaly related to earthquake. Day 41 shows anomaly at VTEC and dTEC, while geomagnetic conditions are quiet on this day, this can be due to aftershocks, further research is needed to look for such changes.
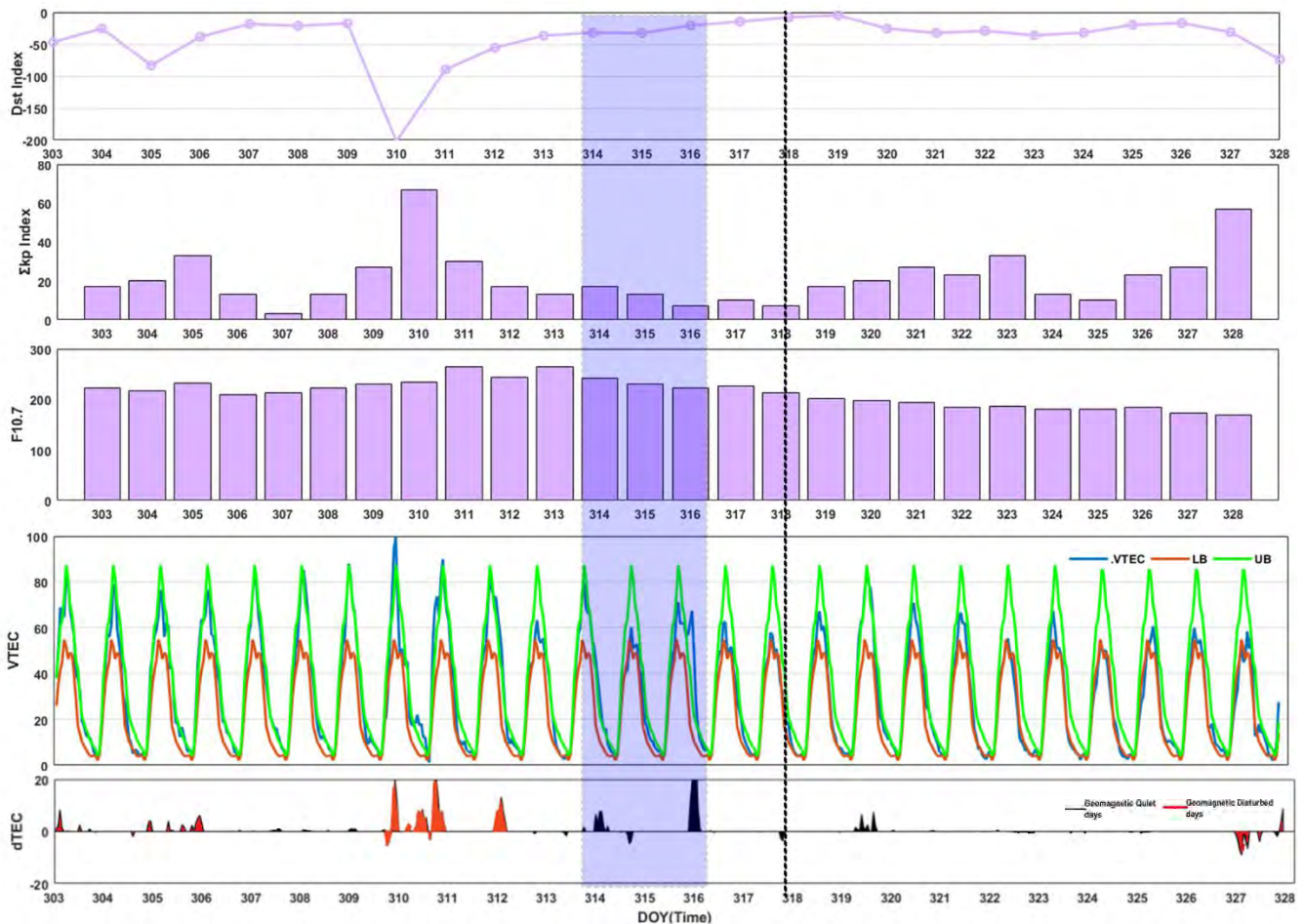

Figure 5.2: Geomagnetic storms indices (a, b, & c) are presented in top 3 panels and bottom 2 panels are representing Temporal VTEC with UB/LB and dTEC of February 7, 2004, Indonesia. Solid dashed line marks earthquake day while blue box represents PEIA days.

5.2.4 April 20, 2006, Russia

The GPS-TEC and geomagnetic indices data for 26 days is processed i.e., 15 days before the main shock, the earthquake day, and 10 days after the event to check for Pre earthquake ionospheric anomalies associated with the earthquake of April 20, 2006. Day 99 and 105 are highly disturbed magnetic days. Figure 5.4 is Graphical analysis of the data, and no observable pre-earthquake ionospheric anomaly can be seen before the earthquake.
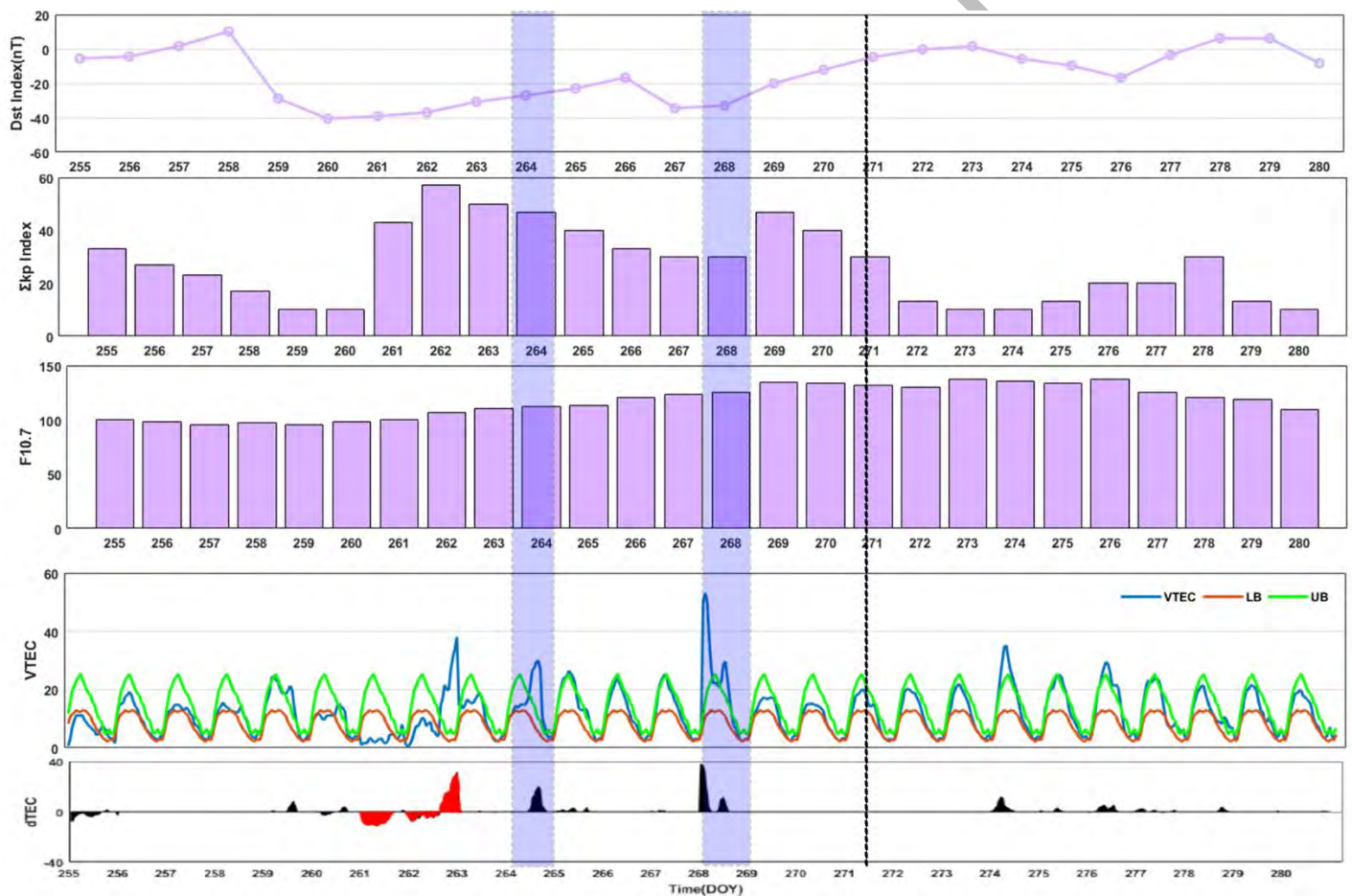

Figure 5.4: Geomagnetic storms indices (a, b, & c) are presented in top 3 panels and bottom 2 panels are representing Temporal VTEC with UB/LB and dTEC of April20, 2006, Russia. Solid dashed line marks earthquake day while blue box represents PEIA days.

5.2.5 October 23, 2011, Turkey

Ionospheric anomalies are found in GPS-TEC data prior to the earthquake of Turkey, October 23, 2011. Before the main shock, the geomagnetic storm indices were quiet. The VTEC and dTEC values present positive TEC anomaly on earthquake day (296) and five to six days (290-291) prior to the main shock are greater than 5 TECU and 3 TECU respectively, that can be seen in Figure 5.5. These results are synchronized with the results of Senturk and collogues who had worked on this earthquake previously (Senturk et al., 2019). During the EQ preparation stage, an enormous burst in TEC is caused primarily by the execution of EQ, which spread from the epicenter through the lower atmosphere to the ionosphere. An enhancement in GPS-TEC is observed that is slightly above the upper bound which can be an indication of the pre-earthquake ionospheric anomaly before earthquake of October 23, 2011, Turkey.
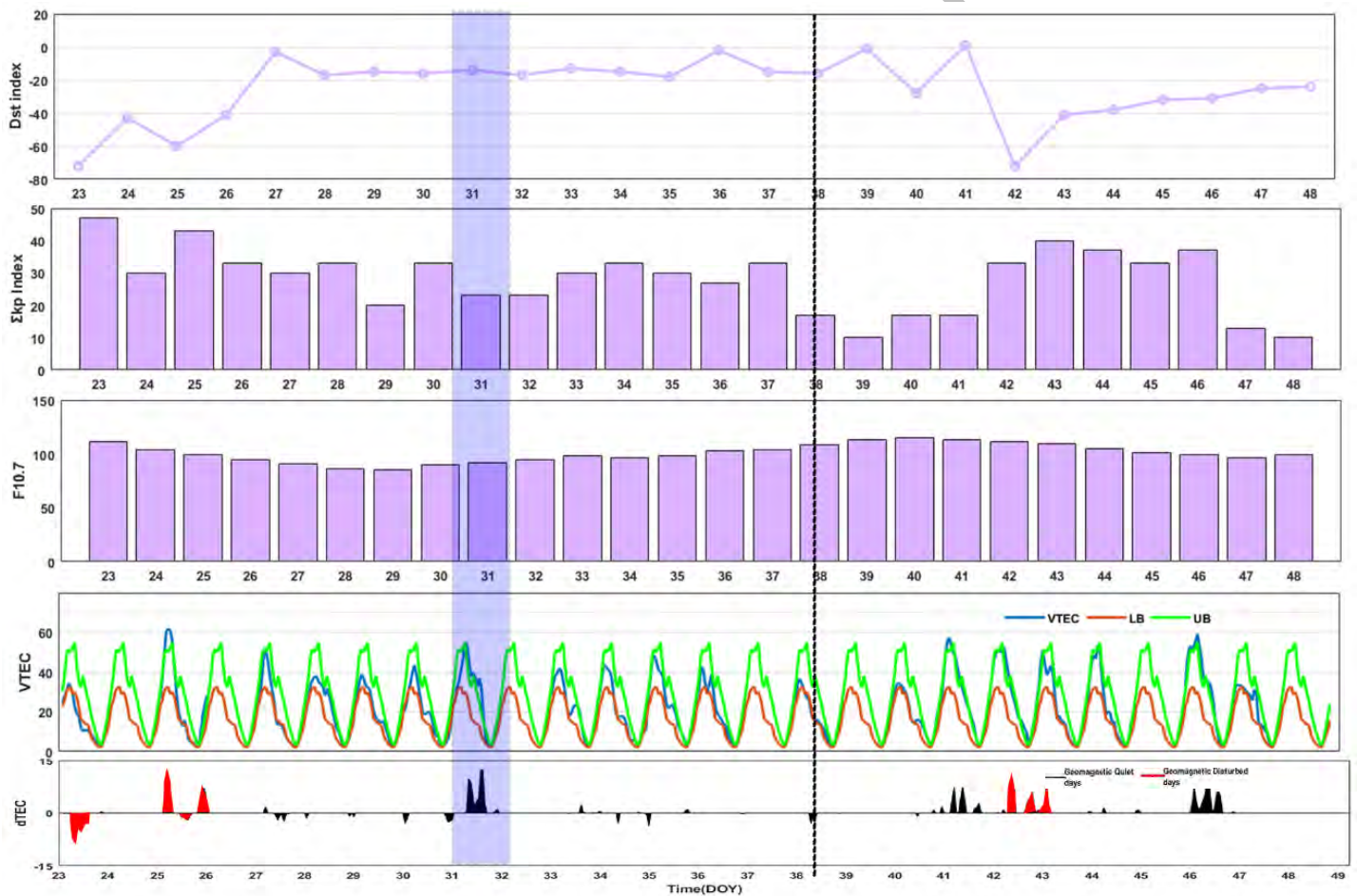

Figure 5.5: Geomagnetic storms indices (a, b, & c) are presented in top 3 panels and bottom 2 panels are representing Temporal VTEC with UB/LB and dTEC October 23, 2011, Turkey. Solid dashed line marks earthquake day while blue box represents PEIA days

5.2.6 September 5, 2012, Costa Rica

Processing of 26 days data for September 5, 2012, earthquake of Costa Rica has been done to observe the pre-earthquake ionospheric anomalies. Geomagnetic conditions are disturbed from day 247 to 249, then gradually deceases afterwards. Positive VTEC anomaly can be seen at day 238 which is further shown at dTEC variation showing 10 TECU above upper bound, Figure 5.6 is representing the graphically analysis of the data. 11 days prior to the earthquake this anomaly has been detected which can be due to ionospheric disturbance.
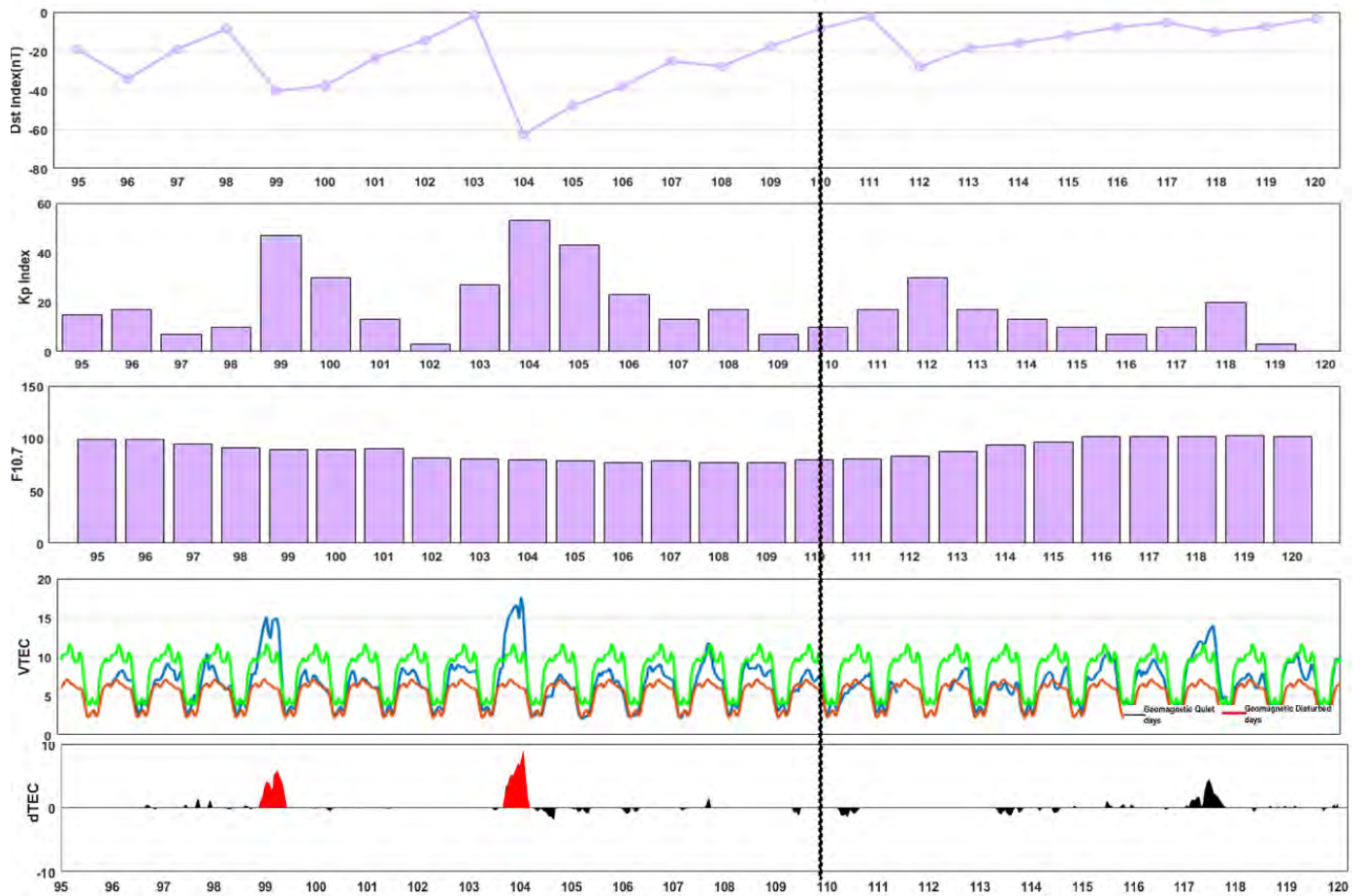

Figure 5.6: Geomagnetic storms indices (a, b, & c) are presented in top 3 panels and bottom 2 panels are representing Temporal VTEC with UB/LB and dTEC of September 5, 2012, Costa Rica. Solid dashed line marks earthquake day while blue box represents PEIA days.

5.2.7 September 24, 2013, Pakistan

GPS-TEC data for 26 days, 15 days prior and 10 days after the earthquake of September24, 2013, Pakistan has been plotted along with upper and lower bound to analyze pre- earthquake ionospheric anomalies. Geomagnetic conditions are quite before the earthquake which can be seen at top three panels of the Figure 5.7. VTEC enhancement has been observed two days (265) before the earthquake which is further verified by dTEC plot showing 5TECU variation above the upper bound. At day 269 there is 10TECU enhancement in anomaly which can be due aftershocks because geomagnetic conditions are quiet.
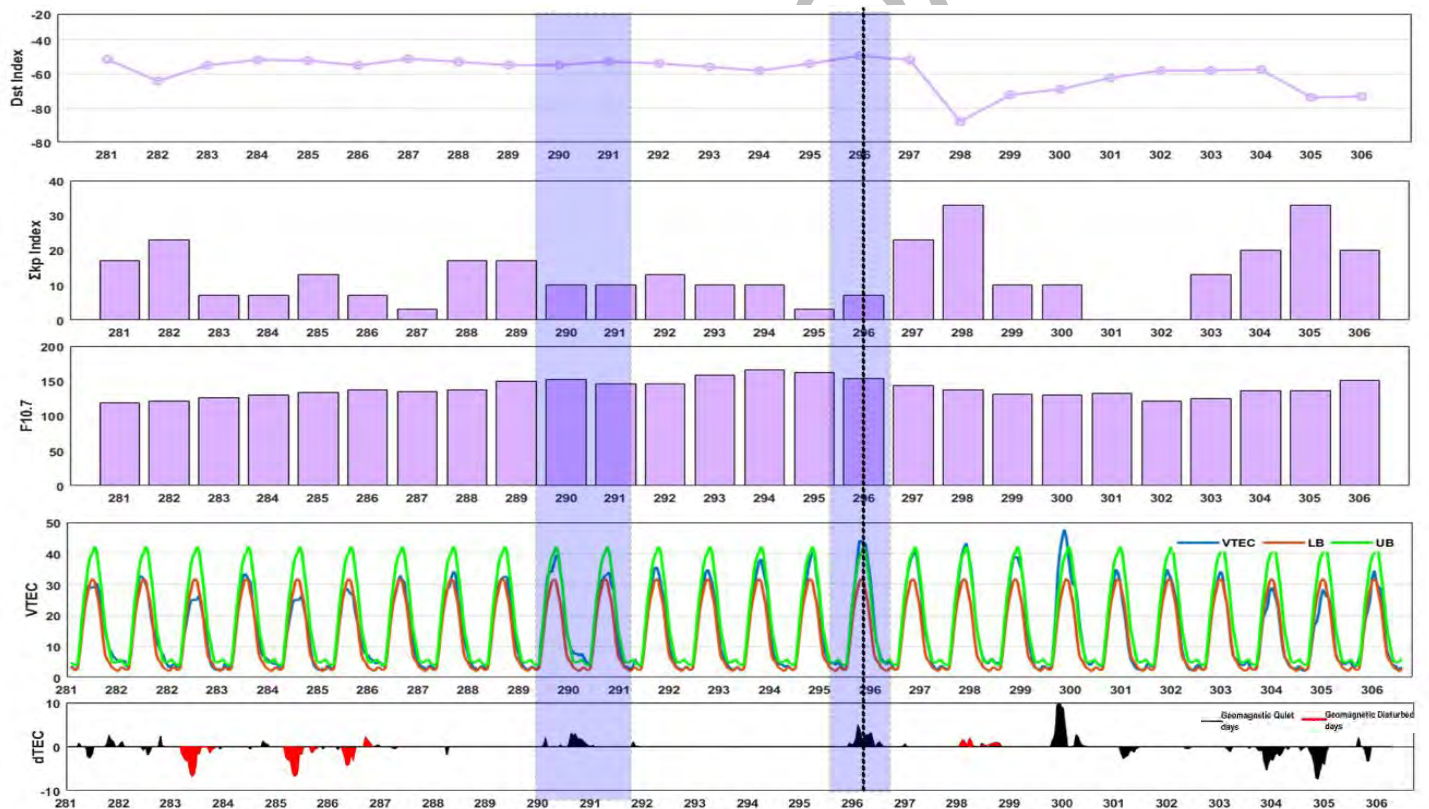

Figure 5.7: Geomagnetic storms indices are presented in top 3 panels (a, b, & c) and bottom 2 panels are representing Temporal VTEC with UB/LB and dTEC of September 24, 2013, Pakistan. Solid dashed line marks earthquake day while blue box represents PEIA days.

5.2.8 April 25,2015, Nepal

GPS-TEC along with dTEC shows very high anomaly for April 25, 2015, Nepal earthquake. The dTEC values for VTEC obtained in the EQ preparation zone on day 113-114 corresponds to one and two days before the event, which is more than 25 TECU while at day 104 which is eleven days prior to the main event shows almost 30TECU above the upper bound, that can be seen at Figure 5.8. These enhancement in VTEC can be an indication of pre-earthquake ionospheric anomalies, where the geomagnetic storm indices are quiet before to the main shock. This huge burst in TEC is mainly the execution of EQ which propagated from the epicenter via lower atmosphere to the ionosphere during the EQ preparation period (Shah and Jin, 2015)
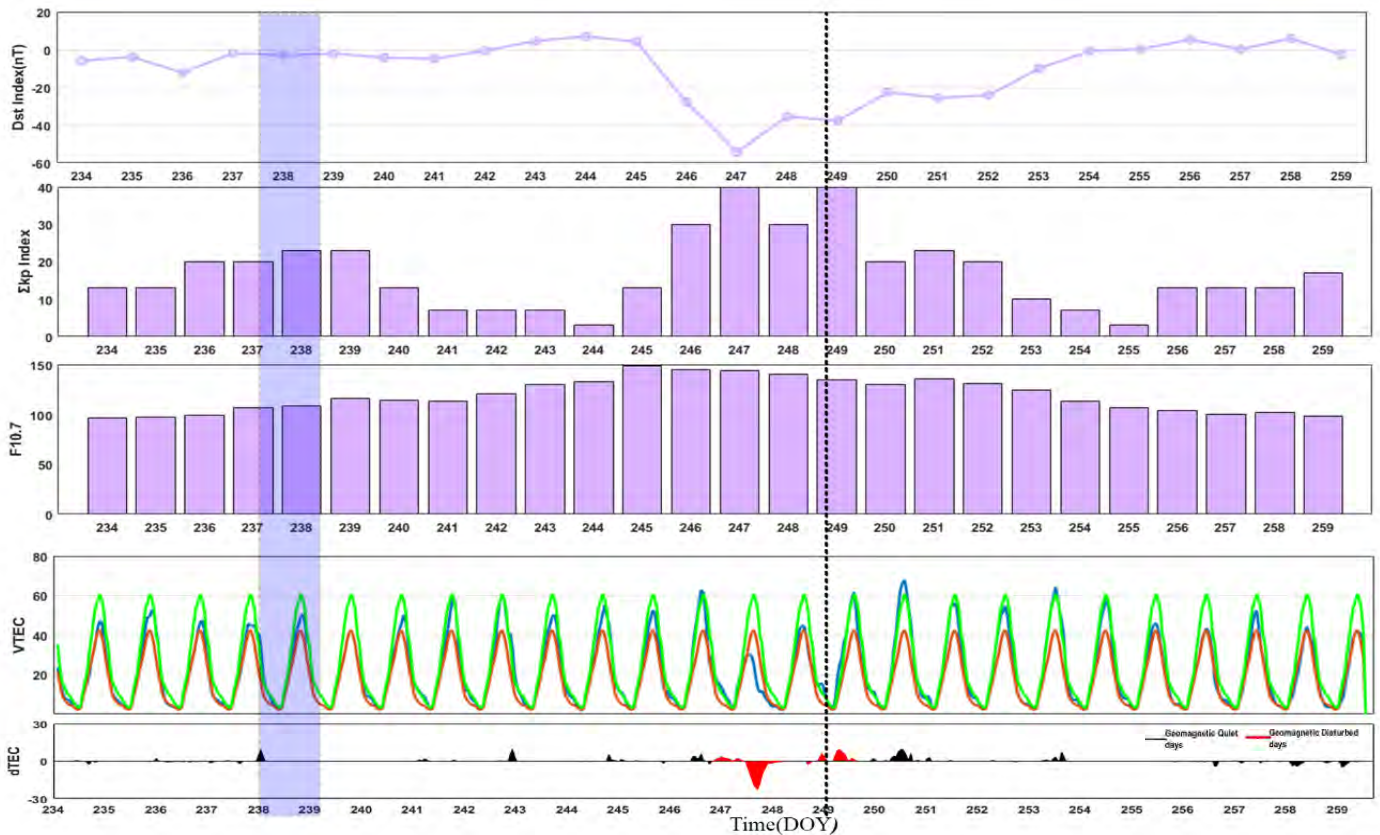

Figure 5.8: Geomagnetic storms indices are presented in top 3 panels (a, b, & c) and bottom 2 panels are representing Temporal VTEC with UB/LB and dTEC of April 25,2015, Nepal. Solid dashed line marks earthquake day while blue box represents PEIA days.

5.2.9 May 12,2015, Nepal

The GPS-TEC along with upper and lower bound has been plotted along with dTEC and geomagnetic indices forMay 12, 2015, Nepal earthquake which can be seen in Figure 5.9. The rapid increment in TEC was also found within 5 days before the M7.3 Nepal EQ, which is more than 20 TECU beyond the upper bound. 5-10 VTEC variations can also be seen from day 125 to 131. These could be the pre-seismic precursor because the execution of the geomagnetic storm is negligible (Kp < 50). On the other hand, the VTEC anomalies are further intensified in the dTEC data. 3 days after the event there is a spike at VTEC while geomagnetic conditions are quite at that day. This can be due to earthquake aftershock, but further research is needed to be done for small magnitude earthquakes to verify this theory
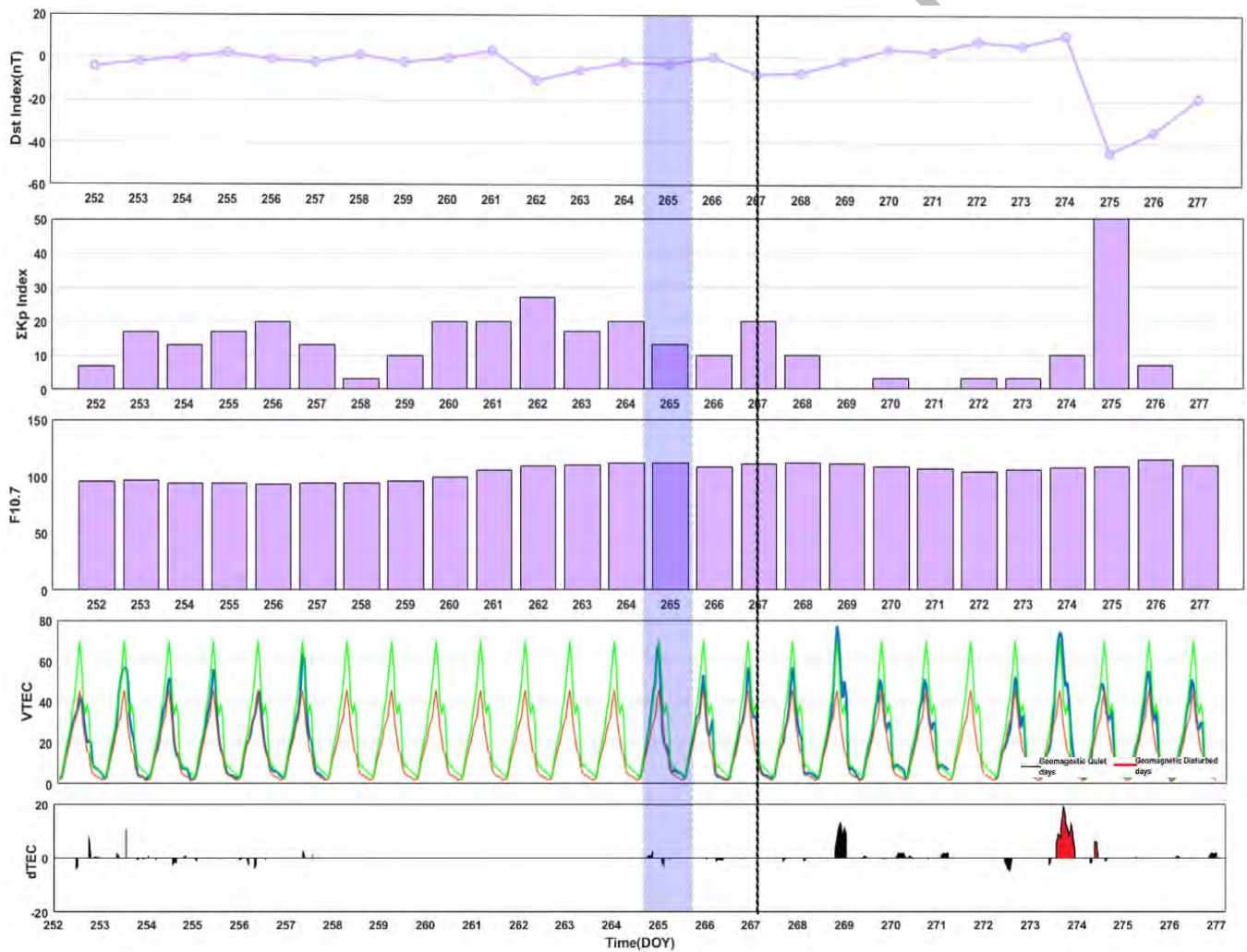

Figure 5.9: Geomagnetic storms indices are presented in top 3 panels (a, b,& c) and bottom 2 panels are representing Temporal VTEC with UB/LB and dTEC of May,12, 2015,Nepal. Solid dashed line marks earthquake day while blue box represents PEIA days.

5.2.10 February 25,2018, Papua New Guinea

Geomagnetic and VTEC data analysis give us an idea of how VTEC variation can happen due to earthquakes.26 days VTEC along with upper bound and lower bound has been plotted to observe PEIAs. Day 46-49 shows 3 to 5 TECU enhancement above upper bound which is seven to ten days prior to the EQ. Day 54 also shows anomalous VTEC values about 6TECU above upper bound which can be seen at Figure 5.10. These can be indication of pre-earthquake ionospheric anomalies because geomagnetic condition quite before the earthquake.
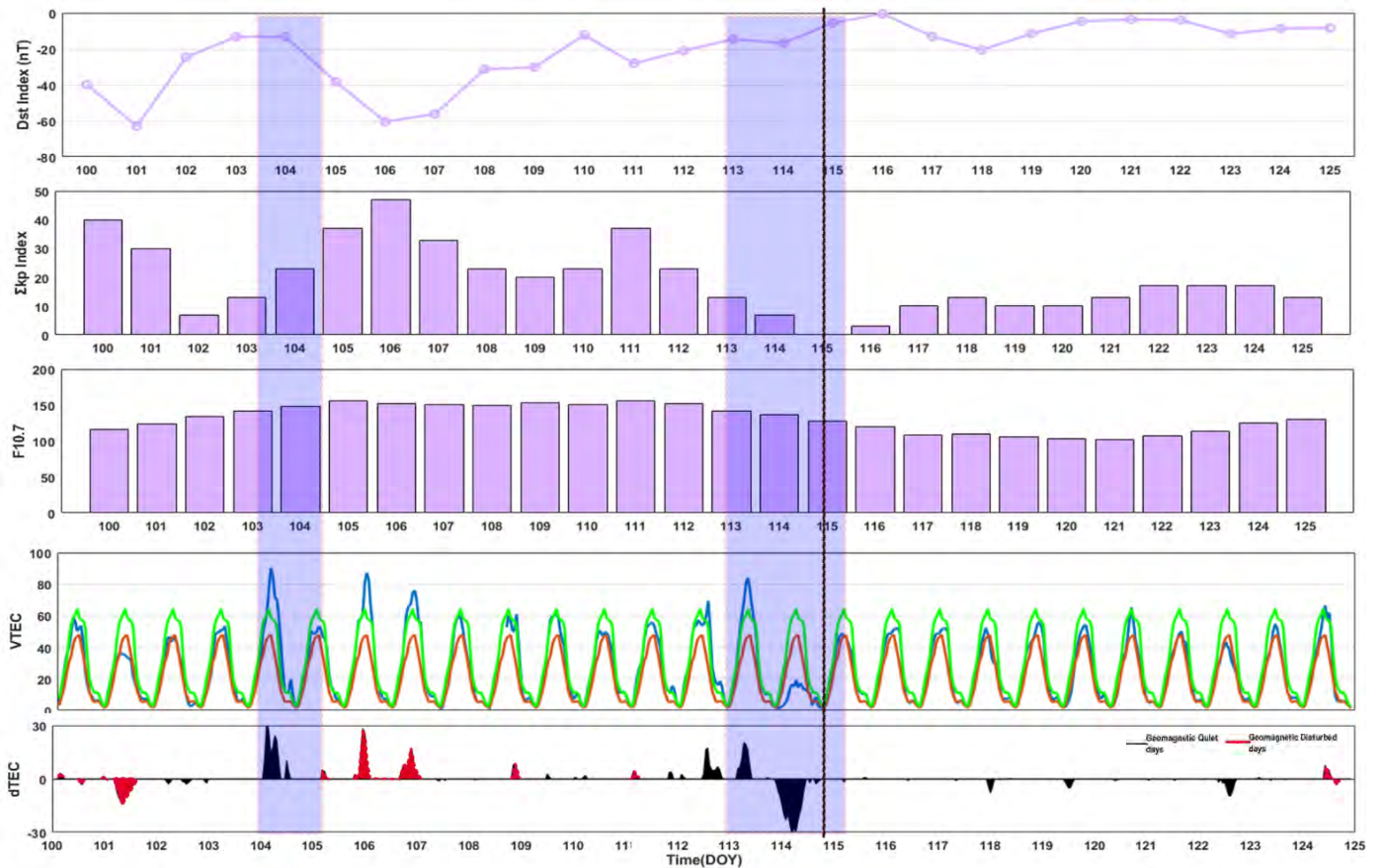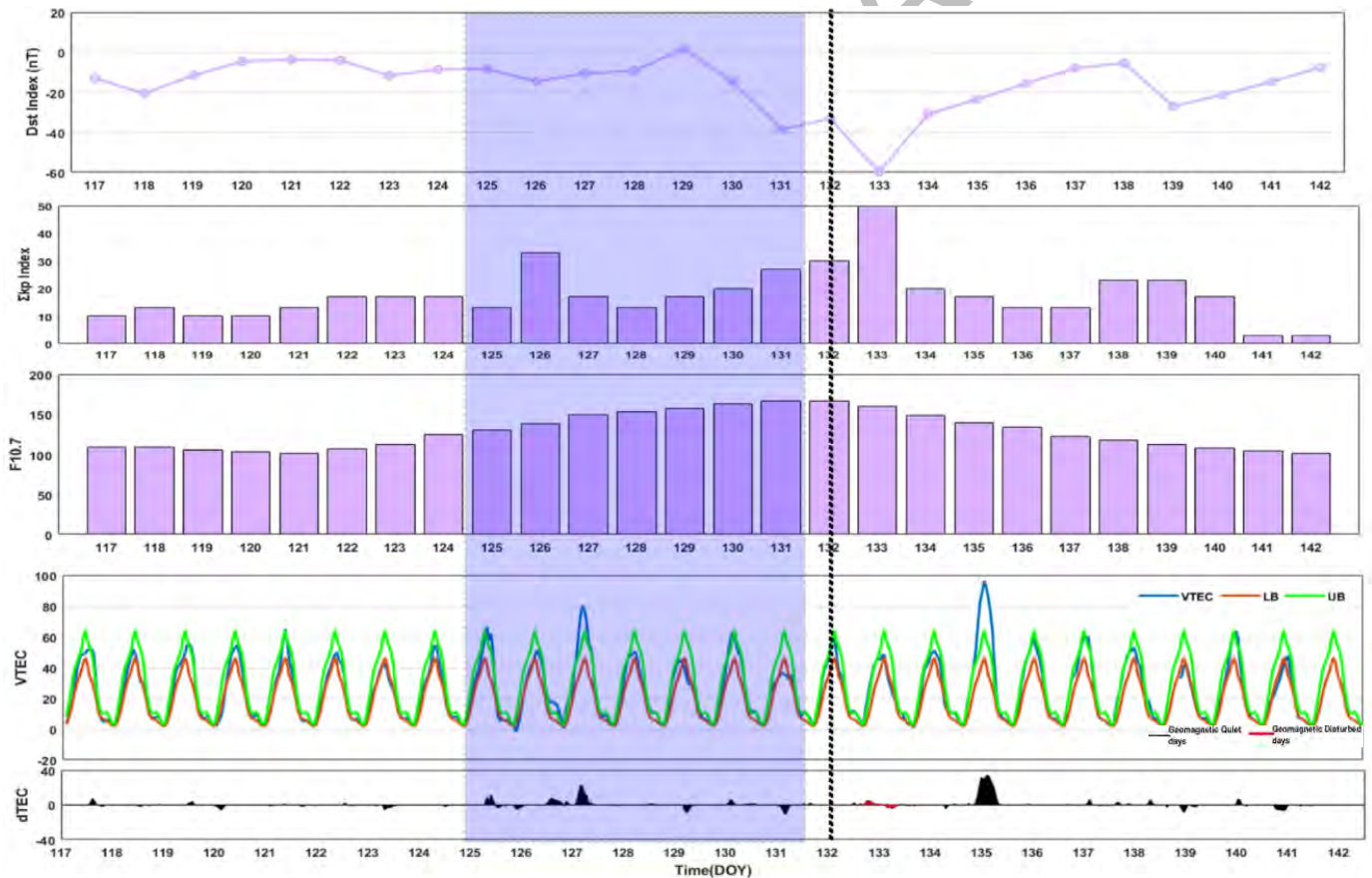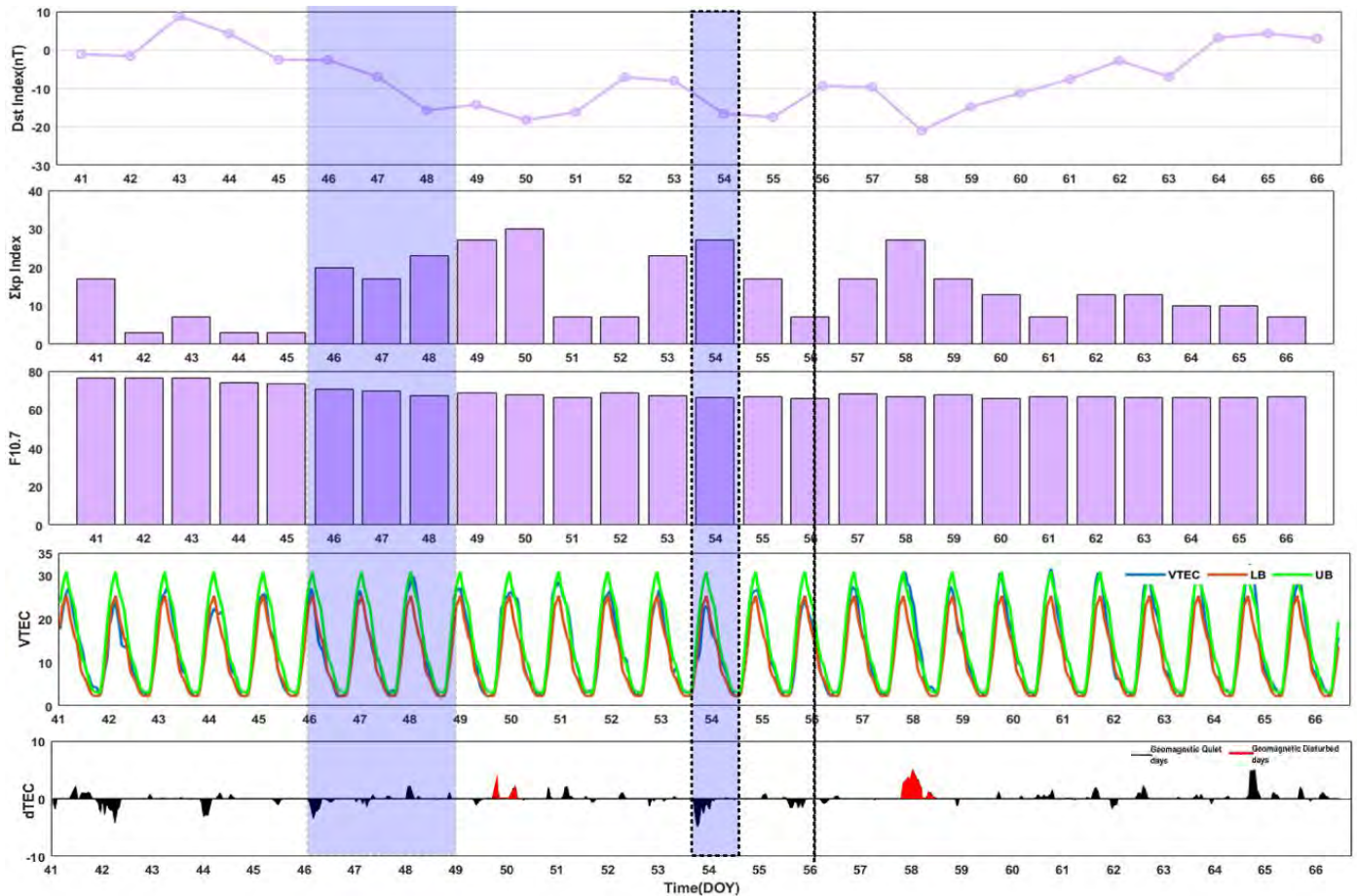

Figure 3.10: Geomagnetic storms indices are presented in top 3 panels (a, b, & c) and bottom 2 panels are representing Temporal VTEC with UB/LB and dTEC of February 25,2018, Papua New Guinea. Solid dashed line marks earthquake day while blue box represents PEIA days.

5.3 Land Surface Temperature Analysis

The behavior of the relevant temperature variations at surface of the earth before and after earthquakes is frequently studied using satellite remote sensing data as probable earthquake precursors. Among the most essential data sources utilized for earthquake forecasting are satellite-derived Land Surface Temperature (LST) products. Thermal Infrared (TIR) bands of the sensors are used to obtain satellite based LST (Sekertekin &Arslan, 2019). A thermal anomaly is an anomalous rise in LST that happens one to ten days before an earthquake and has increases in temperature of at least three to twelve degrees Celsius. It typically goes away a few days following the occurrence (Ahmed et al., 2019).

To evaluate whether the LST could be an earthquake precursor, many experts have investigated LST anomalies (Chen et al., 2006; shah et al., 2021). In this research LST analysis is done for earthquake of September 24, 2013, in Pakistan. LST analysis is done as a secondary work to look for temperature anomalies before an earthquake. Cloud free MODIS data has been used for research purpose. Along with that, Mod11A1 product has very high temporal resolution and comparatively less spatial resolution. For daily temperature variation MOD11A1 product is the best product because of high temporal resolution.

5.3.1 LST Maps for September 2013 Earthquake in Pakistan

This study used the Moderate Resolution Imaging Spectroradiometer (MODIS) satellite's night time Land Surface Temperature (LST) data to analyses abnormal changes 15 day before and 10 days after the Pakistan earthquake on September 24, 2013, with magnitude of 7.7. These maps been generated using ArcGIS software with the help of spatial analysis tool which is immensely helpful in raster data analysis.

Temperature value of each day at epicenter have been noted down and a graph is plotted against days of the year to quantitively represent the temperature variations. The research is focused on spatial and temporal variation of LST only at epicenter. Figure 5.11 represents the LST maps of 26 days from 252 to 277 days of the year with earthquake's epicenter having latitude 26.9° N, and longitude of 65.5° E. Quantitative analysis has been

done for 26 values of LST for each day which is graphically represented at Graph 1. This investigation identified pre- and post-earthquake behaviors as an increase in temperature within 4 days (DOY 263) of the major shock which can be noted as 29.5 Celsius which is 3 Celsius higher than average temperature. This demonstrates how LST anomalies can be used to detect potential earthquake anomalies. This is basic data analysis technique, but more research and techniques needed to be applied to these products to get better results. In raster calculator the following formula give LST in Degree Celsius.

LST(Celsius)= (MOD11A1*scaling factor)-Absolute zero
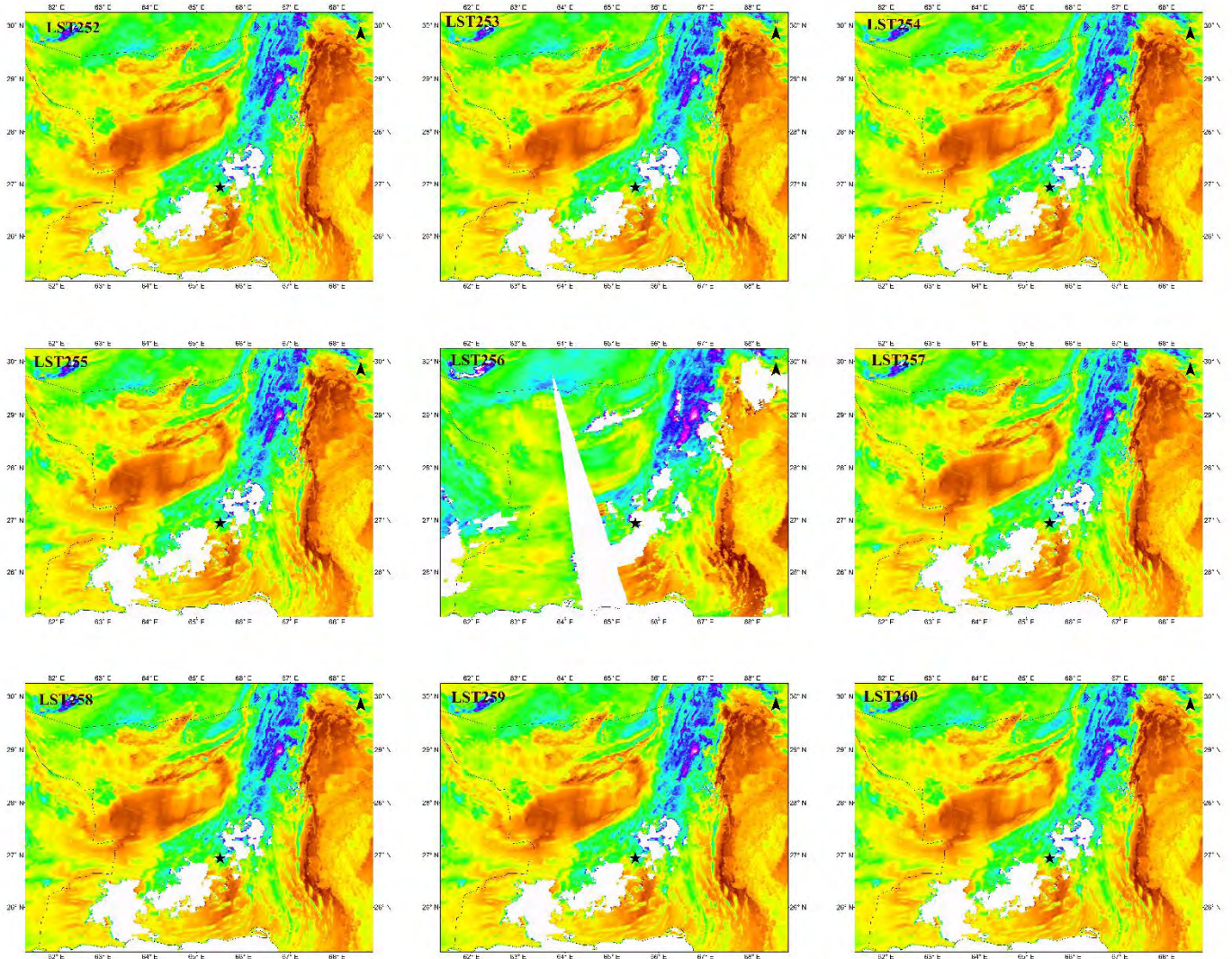
Figure 5.11: MODIS land surface temperature Maps for 26 days (252-277 DOY) for September 24, 2013, earthquake Pakistan.

Graph 1: LST variation graph with 263 days being higher than average LST.

CHAPTER 6

Discussion and Recommendation

6.1 Discussion

Since ancient times, pre-earthquake phenomena have been a major focus of study across a wide range of scientific disciplines; however, in recent decades, a significant effort has been made to investigate these precursory phenomena with the help of observational data. The understanding of various physical features 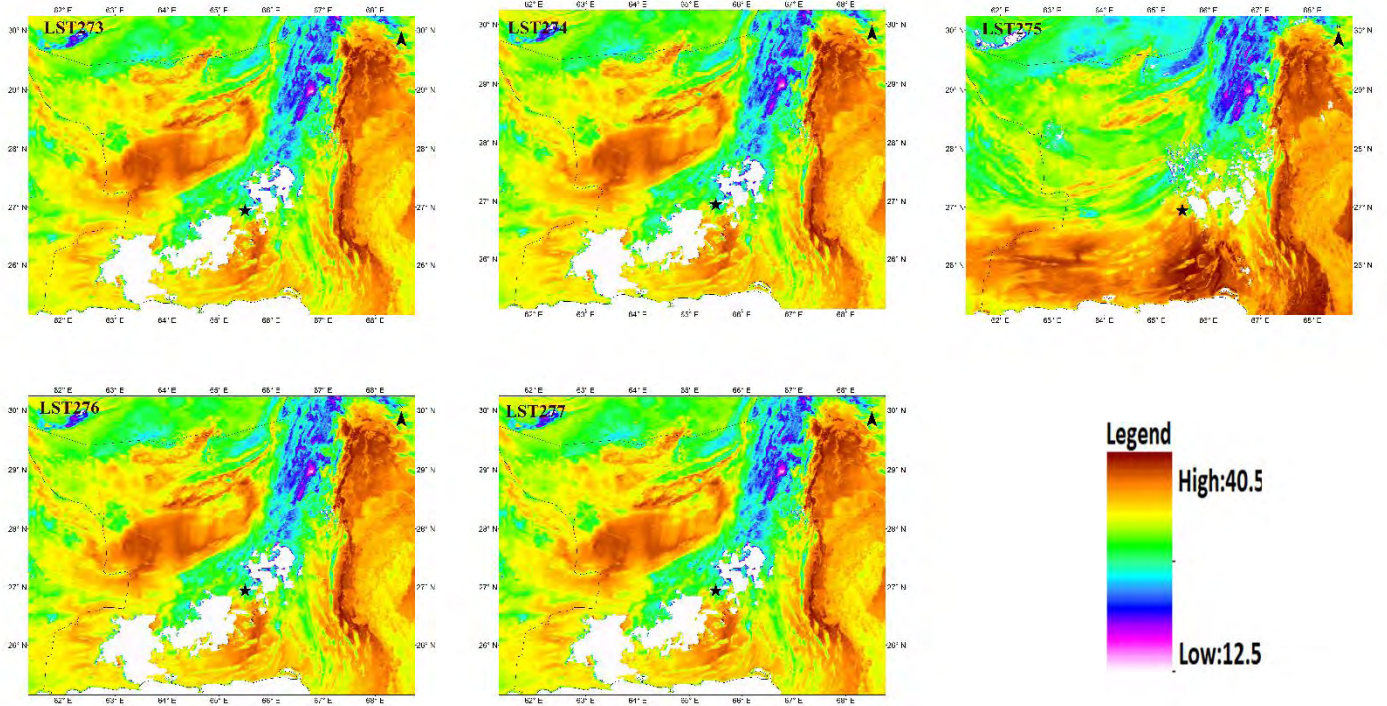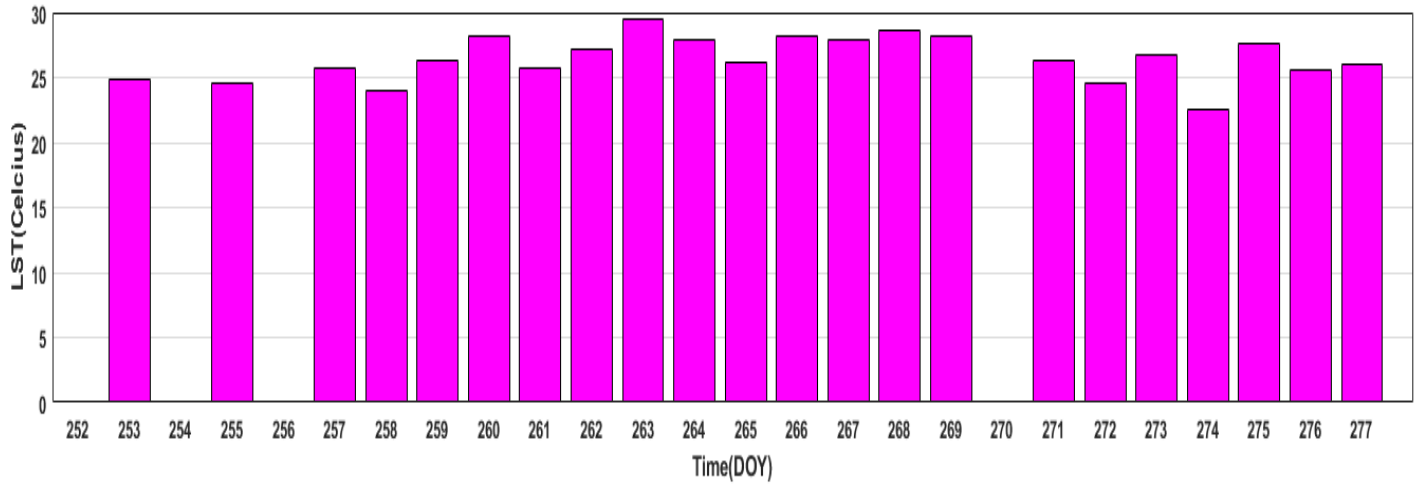describing several components of the earth-atmosphere system especially ionosphere, considering that such precursory phenomena can be used to forecast future earthquakes. The worldwide networks of ground based GNSS receivers provide a great opportunity for global monitoring of the state of the environment close to the Earth hence pre-earthquake ionospheric studies. GPS-TEC data has been used to study the pre-earthquake ionospheric anomalies.

This research investigates the temporal variation for potential ionospheric anomalies linked to EQs (Mw > 7.0 & Depth<50km) worldwide. The study yields a significant link between GNSS TEC disturbances over the epicenter within earthquake preparation zone. TEC from various IGS stations within Dobrovolsky's radius at different hours for all the earthquakes, 15 days before and 10 days after the main earthquake have been collected. Along with these solar geomagnetic conditions were also taken into care with the help of geomagnetic indices (Dst, Kp, & F10.7) and are plotted along with VTEC data to analyze geomagnetic condition at the time of the earthquake.

Ionospheric data reveal anomalies after statistical examination of the VTEC data. Nine out of ten earthquakes exhibit substantial VTEC features within a window of 1 to 11 days, and these anomalies disappear after the earthquake occurs, which is consistent with the predicted outcomes. Out of which six earthquakes shows PEIA 2 days before the event. The execution of EQ, which stretched from the epicenter through the lower atmosphere to the ionosphere several days before the main seismic shock, is likely what caused the large surge in TEC that occurred during the EQ preparation stage. Four earthquakes also exhibit VTEC enhancement six to seven days before the earthquake. These recurrent

trends can serve as reliable earthquake forecasting markers. Three earthquakes also show PEIA 10 to 11 days prior to the incident. Energy emission 11 days prior to an event can be a good and early indicator of upcoming earthquake, the information if used wisely can help human being from big disasters but it is a topic of controversy so far.

Likewise, Land surface temperature maps are used as secondary data to look for temperature variations before large earthquake. LST maps have been developed for 15 days before and 10 days after the earthquake. LSTs at epicenter have been noted down and daily temperature graphs have been developed to see LST variation at the epicenter.

Conclusion

Extensive research has been done on GPS-TEC data along with Geomagnetic indices on 10 shallow depth earthquakes with magnitude equal to or greater than 7, geographically located at different places on the earth. Dst, Kp and F10.7 data has been used to monitor geomagnetic condition during the study duration. GPS-VTEC and dTEC variations is helpful in analyzing possible anomalies with respect to the earthquakes. The statistically analysis on selected earthquakes presents positive anomalies before maximum earthquakes which synchronized with our predicted results. LST temperature variations are also complimenting with idea of rise in temperature before large earthquakes. The ionosphere is sensitive to the energy released during earthquake evolution, especially, Shallow depth earthquakes with high magnitude disturbs the ionosphere due to execution of energy from epicenter before the earthquakes. Quantitative analysis of the selected earthquake has been shown in table 6.1.

Table 6.1: Detail of Required Earthquakes.

Date	Magnitude	Depth (Km)	Region	GNSS Station	PEIA	PEIA Days before the event
11/14/2001	7.8	33	China	WUH	yes	2-4
9/27/2003	7.3	10	Russia	IRKJ	yes	2 & 6
2/7/2004	7.3	16	Indonesia	LAE	yes	7
4/20/2006	7.6	22	Russia	PETS	No	-
10/23/2011	7.1	18	Turkey	ANK	yes	1 & 6
9/5/2012	7.6	35	Costa Rica	MANA	yes	11
9/24/2013	7.7	35	Pakistan	YIBL	yes	2
4/25/2015	7.8	15	Nepal	LCK	yes	1-2 & 11
5/12/2015	7.3	8.22	Nepal	LHAZ	yes	1-6
2/25/2018	7.5	25.21	PNG	PNGM	yes	2 & 10-11

Recommendation

The study merely offers initial statistical results; more investigation, utilizing more TEC and other observational data, is necessary. The need for setting up a network of various stations and devices in a seismically active area, including GNSS receivers, radon, temperature, and atmospheric electric field sensors highlighted. Such conditions will not only help researchers to understand the ionosphere-lithosphere-atmosphere dynamics but can helps reduce risk of earthquake destructions if required results are forecasted timely. At the end of the research there are few suggestions regarding the data used and methodologies that can help in enhancement of the work for future studies.

1. More IGS station data for single earthquake is needed to be used to verify the work.
2. The ionospheric parameters' variation is likely to be visible at the station nearest to the epicenter that is why it is recommended to take data of station that is near to epicenter.
3. These techniques can be used for lower magnitude earthquakes as well.
4. Cloud cover free MODIS data can be used to study the phenomena spatially along with temporal variations.
5. Other techniques are required to study earthquakes with epicenter at offshore.
6. Earthquake forecasting will be more authenticated with more parameters like LST, VEF, ionosphere, radon gas analysis and so on.

References

Ahmad, N., Barkat, A., Ali, A., Sultan, M., Rasul, K., Iqbal, Z., & Iqbal, T. (2019). Investigation of spatio-temporal satellite thermal IR anomalies associated with the Awaran earthquake (Sep 24, 2013; M 7.7), Pakistan. Pure and Applied Geophysics, 176(8), 3533–3544.

Ambraseys, N. N., & Douglas, J. (2004). Magnitude calibration of north Indian earthquakes. Geophysical Journal International, 159(1), 165-206

Artru, J., Lognonné, P., & Blanc, E. (2001). Normal modes modelling of post-seismic ionospheric oscillations. Geophysical Research Letters, 28(4), 697-700.

Barrile, V., Cacciola, M., & Cotroneo, F. (2006). Multipath reduction of GPS measures through heuristic techniques of compensation. Session 3P7 Modeling and Inverse Problems, 989.

Calais, E., & Minster, J. B. (1995). GPS detection of ionospheric perturbations following the January 17, 1994, Northridge earthquake. Geophysical Research Letters, 22(9), 1045-1048.'

Calais, E., & Minster, J. B. (1998). GPS, earthquakes, the ionosphere, and the Space Shuttle. Physics of the Earth and Planetary Interiors, 105(3-4), 167-181.

Catherine, J. K., Maheshwari, D. U., Gahalaut, V. K., Roy, P. N. S., Khan, P. K., & Puviarasan, N. (2017). Ionospheric disturbances triggered by the 25 April 2015 M7. 8 Gorkha earthquake, Nepal: Constraints from GPS TEC measurements. Journal of Asian Earth Sciences, 133, 80-88.

Chen, YI., J.YLiu,YB.Tsai,and C.S.Chen (2004), Statistical tests for pre-earthquake ionospheric anomaly, Terr.Atmos. Oceanic Sci., 15, 385-3

Davies, K., & Baker, D. M. (1965). Ionospheric effects observed around the time of the Alaskan earthquake of March 28, 1964. Journal of Geophysical Research, 70(9), 2251-2253.

Baker, D. N., Akasofu, S. I., Baumjohann, W., Bieber, J. W., Fairfield, D. H., Hones Jr, E. W., ... & Moore, T. E. (1984). Substorms in the magnetosphere. NASA Reference Publication, 1120, 8-1.

Ding, F., Wan, W., Xu, G., Yu, T., Yang, G., & Wang, J. S. (2011). Climatology of medium scale traveling ionospheric disturbances observed by a GPS network in central China. Journal of Geophysical Research: Space Physics, 116(A9).

Dobrovolsky, I. P., Zubkov, S. I., & Miachkin, V. I. (1979). Estimation of the size of earthquake preparation zones. Pure and applied geophysics, 117(5), 1025-1044.

Drachev, S. S., Malyshev, N. A., & Nikishin, A. M. (2010, January). Tectonic history and petroleum geology of the Russian Arctic Shelves: an overview. In Geological society, London, petroleum geology conference series (Vol. 7, No. 1, pp. 591-619). Geological Society of London.

Emanov, A. F., Emanov, A. A., & Fateev, A. V. (2021). Seismotectonic Features of the Spatial Volumetric Structure of Faults Activated with Chuy Earthquake M s= 7.3 Occurred on September 27, 2003, in Mountain Altai (Russia): Results of the Study of the Upper-Crustal Focal Area. Geotectonics, 55(2), 240-249.

Forbes, J. M., Palo, S. E., & Zhang, X. (2000). Variability of the ionosphere. Journal of Atmospheric and Solar-Terrestrial Physics, 62(8), 685-693.

Freund, F. (2011). Pre-earthquake signals: Underlying physical processes. Journal of Asian Earth Sciences, 41(4-5), 383-400.

Freund, F., & Sornette, D. (2007). Electro-magnetic earthquake bursts and critical rupture of peroxy bond networks in rocks. Tectonophysics, 431(1-4), 33-47.

Ghaffari Razin, M. R., Moradi, A. R., & Inyurt, S. (2021). Spatio-temporal analysis of TEC during solar activity periods using support vector machine. GPS Solutions, 25(3), 1-13.

Hall, R. (2009). Indonesia, geology. Encyclopedia of Islands, Univ. California Press, Berkeley, California, 454-460.

Heki, K., & Enomoto, Y. (2013). Preseismic ionospheric electron enhancements revisited. Journal of Geophysical Research: Space Physics, 118(10), 6618-6626.

Heki, K., & Ping, J. (2005). Directivity and apparent velocity of the coseismic ionospheric disturbances observed with a dense GPS array. Earth and Planetary Science Letters, 236(3-4), 845-855.

Holliday, J. R., Nanjo, K. Z., Tiampo, K. F., Rundle, J. B., & Turcotte, D. L. (2005). Earthquake forecasting and its verification. Nonlinear Processes in Geophysics, 12(6), 965-977.

Jin, S. G., Jin, R., & Li, D. (2016, February). Assessment of BeiDou differential code bias variations from multi-GNSS network observations. In Annales Geophysicae (Vol. 34, No. 2, pp. 259-269). Copernicus GmbH.

Jin, S. G., Wang, H. P., & Zhu, W. Y. (2004). Realtime prediction and monitoring of the total ionospheric electron content by means of GPS observations. Chinese Astronomy and Astrophysics, 28(3), 331-337.

Jin, S., Jin, R., & Li, J. H. (2014). Pattern and evolution of seismo-ionospheric disturbances following the 2011 Tohoku earthquakes from GPS observations. Journal of Geophysical Research: Space Physics, 119(9), 7914-7927.

Klinger, Y., Xu, X., Tapponnier, P., Van der Woerd, J., Lasserre, C., & King, G. (2005). High-resolution satellite imagery mapping of the surface rupture and slip distribution of the M w~ 7.8, 14 November 2001 Kokoxili earthquake, Kunlun fault, northern Tibet, China. Bulletin of the Seismological Society of America, 95(5), 1970-1987.

Klobuchar, J. A. (1987). Ionospheric time-delay algorithm for single-frequency GPS users. IEEE Transactions on aerospace and electronic systems, (3), 325-331.

Klotz, S. and N. L. Johnson, (Eds.): Encyclopedia of Statistical Sciences, John Wiley and Sons, 1983.

Kutiev, I., Otsuka, Y., Saito, A., & Tsugawa, T. (2007). Low-latitude total electron content enhancement at low geomagnetic activity observed over Japan. Journal of Geophysical Research: Space Physics, 112(A7).

Liu, C., Zheng, Y., Xiong, X., Wang, R., López, A., & Li, J. (2015). Rupture processes of the 2012 September 5 M w 7.6 Nicoya, Costa Rica earthquake constrained by improved geodetic and seismological observations. Geophysical Journal International, 203(1), 175-183.

Liu, J. Y., Chuo, Y. J., Shan, S. J., Tsai, Y. B., Chen, Y. I., Pulinets, S. A., & Yu, S. B. (2004, April). Pre-earthquake ionospheric anomalies registered by continuous GPS TEC measurements. In Annales Geophysicae (Vol. 22, No. 5, pp. 1585-1593). Copernicus GmbH.

Liu, Jann Yen, Y. J. Chuo, S. J. Shan, Y. B. Tsai, Y. I. Chen, S. A. Pulinets, and S. B. Yu. "Pre-earthquake ionospheric anomalies registered by continuous GPS TEC measurements." In Annales Geophysicae, vol. 22, no. 5, pp. 1585-1593. Copernicus GmbH, 2004.

Liu, L., Wan, W., Chen, Y., & Le, H. (2011). Solar activity effects of the ionosphere: A brief review. Chinese Science Bulletin, 56(12), 1202-1211.

Madlazim. (2012, June). Toward tsunami early warning system in Indonesia by using rapid rupture durations estimation. In AIP Conference Proceedings (Vol. 1454, No. 1, pp. 142-145). American Institute of Physics.

Mjachkin, V. I., Brace, W. F., Sobolev, G. A., & Dieterich, J. H. (1975). Two models for earthquake forerunners. In Earthquake prediction and rock mechanics (pp. 169-181). Birkhäuser, Basel.

Muhammad, S., Iftekar, R., Lamiya, I. B., Khan, W., Sumalani, H., & Bizinjo, A. VALUATION OF AWARAN, BALOCHISTAN, PAKISTAN, EARTHQUAKE: HAZARD ASSESSMENT AND MITIGATION

Parrot, M., Achache, J., Berthelier, J. J., Blanc, E., Deschamps, A., Lefeuvre, F., ... & Villain, J. P. (1993). High-frequency seismo-electromagnetic effects. Physics of the Earth and Planetary Interiors, 77(1-2), 65-83.

Pulinets, S. A., A. D. Legen'ka, T.V Gaivoronskaya, and VK. Depuev (2003), Main phenomenological features of ionospheric precursors of strong earthquakes, J.Atmos. Sol. Terr. Phys., 65, 1337-1347.

Pulinets,S.A.,and K.A.Boyarchuk (2004),Ionospheric Precursors of Earthquakes, Springer, Berlin, Heidelberg and New York, 316pp

Richon, P., Bernard, P., Labed, V., Sabroux, J. C., Beneito, A., Lucius, D., ... & Robe, M. C. (2007). Results of monitoring 222Rn in soil gas of the Gulf of Corinth region, Greece. Radiation measurements, 42(1), 87-93.

Rishbeth, H. (2006). Ionoquakes: Earthquake precursors in the ionosphere? Eos, Transactions American Geophysical Union, 87(32), 316-316.

Rolland, L. M., Vergnolle, M., Nocquet, J. M., Sladen, A., Dessa, J. X., Tavakoli, F., ... & Cappa, F. (2013). Discriminating the tectonic and non-tectonic contributions in the ionospheric signature of the 2011, Mw7. 1, dip-slip Van earthquake, Eastern Turkey. Geophysical Research Letters, 40(11), 2518-2522.

Şentürk, E., & Çepni, M. S. (2018). Ionospheric temporal variations over the region of Turkey: a study based on long-time TEC observations. Acta Geodaetica et Geophysica, 53(4), 623-637.

Shah, M., & Jin, S. (2015). Statistical characteristics of seismo-ionospheric GPS TEC disturbances prior to global Mw≥ 5.0 earthquakes (1998–2014). Journal of Geodynamics, 92, 42-49.

Silina, A. S., E.V Liperovskaya, V A. Liperovsky and C.-VMeister (2001), Ionospheric phenomena before strong earthquakes,Mrt. Hazards Earth Syst. Sci, 1, 113-118

Soloviev, A. A., Gvishiani, A. D., Gorshkov, A. I., Dobrovolsky, M. N., & Novikova, O. V. (2014). Recognition of earthquake-prone areas: Methodology and analysis of the results. Izvestiya, Physics of the Solid Earth, 50(2), 151-168.

Tanyaş, H., Hill, K., Mahoney, L., Fadel, I., & Lombardo, L. (2022). The world's second largest, recorded landslide event: Lessons learnt from the landslides triggered during and after the 2018 Mw 7.5 Papua New Guinea earthquake. Engineering geology, 297, 106504.

Tapan, M., Comert, M., Demir, C., Sayan, Y., Orakcal, K., & Ilki, A. (2013). Failures of structures during the October 23, 2011, Tabanlı (Van) and November 9, 2011, Edremit (Van) earthquakes in Turkey. Engineering Failure Analysis, 34, 606-628.

Tariq, M. A., Shah, M., Hernández-Pajares, M., & Iqbal, T. (2019). Pre-earthquake ionospheric anomalies before three major earthquakes by GPS-TEC and GIM-TEC data during 2015–2017. Advances in Space Research, 63(7), 2088-2099.

Tariq, M. A., Shah, M., Ulukavak, M., & Iqbal, T. (2019). Comparison of TEC from GPS and IRI-2016 model over different regions of Pakistan during 2015–2017. Advances in Space Research, 64(3), 707-718.

Teunissen, P. J. G. (2003). Theory of integer equivariant estimation with application to GNSS. Journal of Geodesy, 77(7-8), 402-410.

Vancutsem, C., Ceccato, P., Dinku, T., & Connor, S. J. (2010). Evaluation of MODIS land surface temperature data to estimate air temperature in different ecosystems over Africa. Remote Sensing of Environment, 114(2), 449-465.

Wan, Z., & Li, Z. L. (1997). A physics-based algorithm for retrieving land-surface emissivity and temperature from EOS/MODIS data. IEEE Transactions on Geoscience and Remote Sensing, 35(4), 980-996.

Wang, S., Xu, C., Li, Z., Wen, Y., & Song, C. (2020). The 2018 Mw 7.5 Papua New Guinea earthquake: A possible complex multiple faults failure event with deep-seated reverse faulting. Earth and Space Science, 7(3), e2019EA000966.

Whitehead, D. W., Staple, B. D., & Daniel, S. L. (1995). Evaluation of potential severe accidents during low power and shutdown operations at Grand Gulf, Unit 1: Summary of results. Volume 1 (No. NUREG/CR--6143-VOL. 1). Nuclear Regulatory Commission.

Xu, C., Xu, X., Dai, F., Wu, Z., He, H., Shi, F., ... & Xu, S. (2013). Application of an incomplete landslide inventory, logistic regression model and its validation for landslide susceptibility mapping related to the May 12, 2008, Wenchuan earthquake of China. Natural hazards, 68(2), 883-900.

Xu, L., & Chen, Y. (2005). Temporal and spatial rupture process of the great Kunlun Mountain Pass earthquake of November 14, 2001, from the GDSN long period waveform data. Science in China Series D: Earth Sciences, 48(1), 112-122.

Zhao, B., Wang, M., Yu, T., Wan, W., Lei, J., Liu, L., & Ning, B. (2008). Is an unusual large enhancement of ionospheric electron density linked with the 2008 great Wenchuan earthquake? Journal of Geophysical Research: Space Physics, 113(A11).

sources:

1 3% match (M. Arslan Tariq, Munawar Shah, M. Hernández-Pajares, Talat Iqbal. "Pre-earthquake ionospheric anomalies before three major earthquakes by GPS-TEC and GIM-TEC data during 2015-2017", Advances in Space Research, 2019)

M. Arslan Tariq, Munawar Shah, M. Hernández-Pajares, Talat Iqbal. "Pre-earthquake ionospheric anomalies before three major earthquakes by GPS-TEC and GIM-TEC data during 2015-2017", Advances in Space Research, 2019

2 1% match (Henry Rishbeth. "Ionoquakes: Earthquake precursors in the ionosphere?", Eos Transactions American Geophysical Union, 2006)

Henry Rishbeth. "Ionoquakes: Earthquake precursors in the ionosphere?", Eos Transactions American Geophysical Union, 2006

3 1% match (Aliihsan Sekertekin, Samed Inyurt, Servet Yaprak. "Pre-seismic ionospheric anomalies and spatio-temporal analyses of MODIS Land surface temperature and aerosols associated with Sep, 24 2013 Pakistan Earthquake", Journal of Atmospheric and Solar-Terrestrial Physics, 2020)

Aliihsan Sekertekin, Samed Inyurt, Servet Yaprak. "Pre-seismic ionospheric anomalies and spatio-temporal analyses of MODIS Land surface temperature and aerosols associated with Sep, 24 2013 Pakistan Earthquake", Journal of Atmospheric and Solar-Terrestrial Physics, 2020

4 1% match (Shuanggen Jin, R, Jin, X, Liu. "GNSS Atmospheric Seismology", Springer Science and Business Media LLC, 2019)

Shuanggen Jin, R, Jin, X, Liu. "GNSS Atmospheric Seismology", Springer Science and Business Media LLC, 2019

5 1% match (student papers from 11-Oct-2022)
Submitted to St Georges - The British International School on 2022-10-11

6 1% match (student papers from 21-Oct-2022)
Submitted to RMIT University on 2022-10-21

7 < 1% match (Internet from 23-Feb-2022)
https://link.springer.com/article/10.1007/s10509-020-03894-3?code=e18435a9-56c9-4d00-a8be-07d8cb876f61&error=cookies_not_supported

8 < 1% match (Internet from 19-Dec-2022)
https://link.springer.com/article/10.1134/S001685210702001X?code=be2134c0-edaa-43b8-bbdb-5bcd0713eabe&error=cookies_not_supported

9 < 1% match (Christina Oikonomou, Haris Haralambous, Sergey Pulinets, Aaknti Khadka et al. "Investigation of Pre-Earthquake Ionospheric and Atmospheric Disturbances for Three